RECONSTRUCTING URBAN CO_2 EMISSIONS UTILISING THE RADIOCARBON COMPOSITION OF TREE RINGS FROM THE WELLINGTON REGION, NEW ZEALAND

BY

INDIA ARABELLA ANSELL

A thesis submitted to Victoria University of Wellington in partial fulfilment of requirements for the degree of Master of Physical Geography

SCHOOL OF GEOGRAPHY, ENVIRONMENT AND EARTH SCIENCES, VICTORIA UNIVERSITY OF WELLINGTON

MAY 2016

ABSTRACT

This study demonstrates the utility of tree ring radiocarbon analysis to quantify a temporal record of recently-added fossil fuel-derived carbon dioxide (CO_{2ff}) in the urban atmosphere, to retrospectively measure emissions and potentially validate local emissions inventories. Currently, there is no internationally recognised method to test emissions inventories against direct atmospheric estimations of CO_{2ff}. With the increasing interest in emissions control legislation, independent and objective research to validate emissions reported by governments and industries is needed.

As CO_{2ff} emissions are completely depleted in radiocarbon (^{14}C), an observed decrease in the ^{14}C content of the atmosphere is mostly due to additions of CO_{2ff}. As trees incorporate CO_2 from the local atmosphere into annual growth rings, it was hypothesised that an urban located tree would reflect emission rates of its local surroundings. Measurements of the ^{14}C content of cellulose were made from the annual tree rings of a Kauri tree (*Agathis australis*), located in the downtown area of the Wellington suburb of Lower Hutt (KNG52). This record was compared with tree rings from two Kauri at a nearby coastal site (NIK19 and NIK23) and the long-term clean air $^{14}CO_2$ record from Baring Head. The clean air Kauri trees, NIK19 and NIK23, demonstrated excellent agreement with the Baring Head atmospheric record, indicating that the trees were accurately sampling the atmosphere. The KNG52 tree, demonstrated good agreement with the clean air record in the early part of the record (with some variability), however, exhibited significantly lower $\Delta^{14}CO_2$ values from the 1980s onward. Calculation of the influence of the terrestrial biosphere on the $^{14}CO_2$ record showed very little impact, determining that the variability seen was due to local additions of CO_{2ff}.

Historic CO_{2ff} emissions were calculated using the $\Delta^{14}CO_2$ measurements from the KNG52 $^{14}CO_2$ record for the period 1972 – 2012. Biosphere correction calculations showed that the biosphere was the dominant influence on the record in the early part of the record (1972 – 1980), with fossil fuel emissions dominating the record from 1980s onward. The observations were compared qualitatively with meteorological data and urban development in the area to assess variability in CO_{2ff}. A minor trend towards lower wind speeds associated with higher levels of CO_{2ff} was identified, indicating that local meteorology may be responsible for 10% change seen in the record. The influence of local development demonstrated some possible relation but a correlation was not significant. The KNG52 CO_{2ff} record was compared with national-level reported liquid (road traffic) emissions from the Carbon Dioxide Information Analysis Centre (CDIAC). The observed KNG52 CO_{2ff} in the tree ring record appeared to increase in tandem with road traffic emissions.

ACKNOWLEDGEMENTS

The completion of this thesis would not have been made possible without the assistance and support of many key people. I would like to express my appreciation to those who dedicated their time and expertise to the completion of this project.

Firstly, a massive thank you to my supervisors. Dr Jocelyn Turnbull, for her unwavering guidance; I am very appreciative for the opportunity to be part of such an interesting area of study, to which I owe Jocelyn. Dr James Renwick, for dedicating his time to supervising, proof-reading and supporting me through my work.

Secondly, I would like to acknowledge my colleagues and lab buddies at GNS Science; Margaret Norris, Jenny Dahl, Jessica Mills, Jeremy Thompson and Cathy Ginnane. Thank you for sharing your technical knowledge, training and support.

Thanks to Dr Gretel Boswijk for her assistance with developing a dendrochronological record that forms the backbone for the data used in this project (and last minute advice). Thank you to Andrea Davies for her assistance in sample preparation.

This has been an equally challenging and rewarding year, which I would have not survived without the constant support of my friends and family. Thank you all for seeing me through what has been an emotional and intellectual voyage.

This research was funded by the New Zealand Government GNS Global Change Through Time program and GNS Strategic Development Fund.

TABLE OF CONTENTS

LIST OF FIGURES

LIST OF TABLES

LIST OF EQUATIONS

ACRONYMS

AMS	Accelerator mass spectrometry
BHD	Baring Head
CDIAC	Carbon Dioxide Information Analysis Centre
GHG	Greenhouse gas
GWRC	Greater Wellington Regional Council
IPCC	Intergovernmental Panel on Climate Change
KNG	52 Kings Crescent (Lower Hutt, NZ), test site for this site
NIC	National Isotope Centre
NIK	19 or 23 Nikau Street (Eastbourne, NZ), background site for this study
UNFCCC	United Nations Framework Convention on Climate Change

CHAPTER 1: INTRODUCTION

Changes in atmospheric composition are directly associated with the growth of world population, industry and technology and the resultant rise in anthropogenic reliance on fossil fuels for transport and electricity generation. Emissions of carbon dioxide (CO_2), a by-product of fossil fuel combustion, are the dominant driver of atmospheric CO_2 increases and current observed global warming. The influence of human activities on the environment has been recognised and there is growing global concern over the unabated rise in atmospheric CO_2 and its associated consequences. Reliable emissions reporting is crucial for enabling local policy makers to instigate the best strategies for reducing emissions. However, currently, carbon emissions reporting is assessed only by "bottom-up" methods that involve reporting of economic data, which aggregate disparate local statistics, producing potentially unrepresentative data (Nisbet & Weiss, 2010). As such, an independent and objective method to validate the emissions reported by governments and industries is essential to ensure accurate emissions estimates are quantified and appropriate reduction strategies can be put in place (Gurney, 2013).

Polar ice-core records show that current atmospheric concentrations of greenhouse gases (GHGs), namely carbon dioxide (CO_2), methane (CH_4) and nitrous oxide (N_2O), exceed any level measured for at least the last 800,000 years (Loulergue et al., 2008; Lüthi et al., 2008; Schilt et al., 2010). Furthermore, the average rate of increase of these gases observed over the past century exceeds any observed rate over the previous 20,000 years (Joos & Spahni, 2008). Due to what is known as the 'greenhouse effect', increased levels of atmospheric GHGs leads to greater absorption of infrared radiation emitted from the Earth's surface and hence, greater re-radiation back down to the surface. This phenomenon has consequently caused a rise in ocean and near-surface air temperatures. Since the industrial revolution in 1750 AD, there has been a marked increase in the atmospheric CO_2 concentration (Tans & Keeling, 2016), a direct result of an increased reliance on fossil fuel combustion for energy production. Thus, CO_2 emissions, and the associated perturbation of the Earth's radiation budget, are recognised as the most significant driver of global warming and consequently, climate change (Ciais et al., 2013).

The role anthropogenic-driven activities have in climate change has been recognised in the policy realm and there are various political bodies working to address this issue and to develop emissions reduction schemes. Currently, carbon emissions reporting is based on "bottom-up" methods that rely on economic data and self-reporting by industries (IPCC, 2006). Inventory tabulations are produced only every few years and must be extrapolated to the year of analysis potentially leading

to large uncertainties. These techniques also lack understanding of the magnitude and mechanisms of carbon exchange with terrestrial biosphere, which is needed to accurately predict the rate of atmospheric CO_2 change into the future. An ideal method of C_{ff} quantification would obtain measurements in real time for a variety of spatial scales. This would allow improved estimates of fossil fuel emissions for regulatory efforts.

The use of an independent and objective method to validate emissions inventories is needed to enable policy makers to develop the best strategies for reducing emissions at the international, national and local scale. Recent studies have utilised the radiocarbon (^{14}C) method as an unambiguous tracer for fossil fuel CO_2 emissions that successfully distinguishes between fossil and non-fossil sources of CO_2 (van der Laan et al., 2010; Turnbull et al., 2011a). Fossil emissions are completely depleted in radiocarbon (Δ_{ff} = -1000‰), thus they can be easily distinguished from other sources of CO_2 such as heterotrophic respiration, biomass burning and plant respiration, which have a radiocarbon content close to that of the atmosphere ($\Delta^{14}C$ = ~29‰; Turnbull et al., 2014a). Standard techniques use measurements of ^{14}C in combination with measurements of CO_2 concentration in air samples to determine the "fraction" of fossil fuel component of CO_2. This method is usually performed on air samples collected in flasks or absorbed in sodium hydroxide (NaOH).

Measurement of the radiocarbon content of urban tree rings has been utilised at individual sites and has the benefit of retrospectively evaluating local fossil fuel CO_2 emissions, which cannot be addressed with current networks of CO_2 monitoring stations. In combination with atmospheric transport models it could be possible to translate the measured fossil fuel CO_2 concentrations into estimates of regional fluxes.

1.1 Aims and objectives

This research aims to demonstrate the utility of tree ring radiocarbon analysis as an accurate method of quantifying atmospheric $\Delta^{14}CO_2$ measurements to examine the drivers of local variability of CO_2, such as:

1. Historic contributions of fossil fuel CO_2 and heterotrophic respiration to variability in ^{14}C,
2. Additions of CO_{2ff} due to anthropogenic activities.

This will be achieved through the following:

i. A reconstruction of past fossil fuel CO_2 concentrations of the atmosphere based on the radiocarbon content of tree rings collected from the Wellington region,
ii. Use of historical meteorological data, to gain an understanding of the regional CO_2 flux in the area,
iii. Analysis of localised urban development, attained from an investigation of historical events and aerial photography, will help to understand fluctuations expected to be seen in the fossil fuel CO_2 record.

Currently, there is no internationally recognised method to test emissions inventories against direct atmospheric estimations of fossil fuel CO_2. With the increasing interest in emissions control legislation, particularly post-Paris Agreement, independent and objective research to validate emissions reported by governments and industries is needed. This verification may be essential to a future comprehensive convention of climate change. As such, research based on direct measurement, independent of reporting bias, could prove to be of interest to local policy agencies to inform emissions reduction strategies.

1.2 Thesis layout

A review of the relevant literature, presented in Chapter 2, elaborates on the current understanding of anthropogenic-driven changes in atmospheric composition, the resultant perturbation of the global carbon cycle and distribution of ^{14}C. It also includes a discussion on current techniques used to quantify fossil fuel CO_2 emissions and an overview of existing records of a similar nature to the one presented in this thesis.

An introduction to the study sites, description of sample collection processes, as well as sample preparation and analytical techniques used are provided in Chapter 3. The sample preparation and analysis was completed by the candidate with assistance from Dr Gretel Boswijk, summer student Andrea Davies and laboratory staff at the Rafter Radiocarbon Laboratory.

Chapter 4 presents the tree ring $^{14}CO_2$ record and includes data obtained through analysis. It also includes the calculation of the fossil fuel CO_2 content of the samples. This section briefly discusses the interpretation of the results in relation to meteorology, urban development and established records of CO_2 emissions.

Chapter 5 concludes the findings and highlights implications for the results and potential for future research.

CHAPTER 2: BACKGROUND

2.1 Actions to curb carbon dioxide emissions

2.1.1 International climate change bodies

Due to the potential destructive consequences of current observed climate change, there is a rising global focus on inhibiting the production of anthropogenic CO_2 emissions (and other GHGs), and therefore a drive for world governments to take action. This has led to the instigation of agencies such as the Intergovernmental Panel on Climate Change (IPCC), International Energy Agency (IEA), and United Nations Framework Convention on Climate Change (UNFCCC) that inform on the consequences of climate change and the implementation of emission reduction policies.

The IPCC is the leading international body for the assessment of climate change, established in 1988 by the United Nations Environment Programme (UNEP) and the World Meteorological Organisation (WMO). The organisation's main priority is "to provide the world with a clear scientific view on the current state of knowledge in climate change and its potential environmental and socio-economic impacts" (IPCC, 2016). The IPCC is an intergovernmental body, with 195 member states, that reviews and assess the most recent scientific, technical and socio-economic information produced worldwide – relevant to the understanding of climate change. It does not conduct any research nor does it monitor climate related data or parameters. Instead, the IPCC produces synthesis reports – of which it has published five. The most recent, the fifth assessment report (AR5) was published in 2014 (IPCC, 2014). These reports are used in support of the UNFCCC, which is the main international treaty on climate change. With 197 parties, the UNFCCC is an international environmental treaty with virtual universal membership, making it the only international climate policy venue with broad legitimacy. Established in 1992 to "stabilise greenhouse gas concentrations in the atmosphere at a level that would prevent dangerous anthropogenic interference with the climate system" (UNFCCC, 1992).

In order to confirm a global obligation to reduce GHG emissions and legally commit signatory members to adhere to internationally binding emissions reductions targets, the Kyoto Protocol was adopted in 1997 after the third Conference of Parties (COP 3) to the UNFCCC (UNFCCC, 1998). Nations that were parties to the Kyoto Protocol were required to provide a national Greenhouse Gas Inventory, which detailed the country's 'emissions profile', specifying GHG contributions from emission producing industries, energy supply, transport infrastructure and land use to be reported to the UNFCCC (UNFCCC, 1998). The first commitment period of the Kyoto Protocol started in 2008 and ended in 2012. A secondary commitment period (from 2013 until 2020), the Doha Amendment,

was proposed in 2012, in which 37 countries – excluding New Zealand – have binding targets. Negotiations held at the 20th Conference of the Parties in Lima in 2014 discussed a post-Kyoto framework that would obligate all major polluters to pay for CO_2 emissions.

COP 21, which was held in Paris in December 2015, marked the 21st yearly session of the Conference of Parties to the 1992 UNFCCC and the 11th session of the Meeting of the Parties (CMP 11) to the Kyoto Protocol. The objective of the conference was to achieve a legally binding and universal agreement on climate to "accelerate international sustainable development and advance the 'green economy'" (UNEP, 2015). At the conclusion of the conference on the December 12, the Paris Agreement was adopted by consensus by 195 countries, signifying the first universal climate agreement in history (UNFCCC, 2015). Signatory members agreed to reduce their carbon output "as soon as possible" and to attempt to restrict global warming "to well below 2 degrees C".

Leading up to the conference in Paris, all nations signatory to the UNFCCC were asked to publish an independent draft national contribution to emissions reduction (called "Intended Nationally Determined Contributions", INDCs). The European Union's suggested INDC, for example, was a commitment to a 40% reduction in emissions by 2030 compared to 1990. New Zealand's INDC, submitted in July of 2015, stated a commitment to reduce GHG emissions to 30% below 2005 levels by 2030. The total global suggested commitments were estimated to limit global warming to 2.7 degrees Celsius by 2100 (UNFCCC, 2016). The establishment of the INDCs was intended as a compromise between the "quantified emissions limitation and reduction objective" and "nationally appropriate mitigation actions" that the Kyoto Protocol used to describe the different legally-binding responsibilities of each nation. When a country ratifies the Paris agreement, the submitted INDCs become the first Nationally Determined Contributions (NDC), which will become the first greenhouse gas targets under the UNFCCC that apply equally to both developed and developing countries. As outlined in the Agreement, there will be no outside agency to approve or administer whether nations are adhering to their targets, however, nations will be subject to a common framework of transparency (Article 13; UNFCCC, 2016).

The intention of Article 13 is to ensure an 'enhanced transparency framework for action and support' (UNFCCC, 2016). Nations are required to provide the information needed to track emissions in a national inventory and report progress in achieving their individual NDCs. The way in which progress in achieving NDCs will be verified was highly disputed during the Paris conference, with the majority of countries supporting an independent review of a nations climate change actions. A number of larger developing countries, namely India and China, rejected third-party involvement. To compromise, it was decided that a technical expert group would review the

consistency of information provided and identify areas of improvement. Therefore, the transparency framework, as outlined in Article 13, does include a small level of third-party review, though must be 'facilitative, non -intrusive, non-punitive [in] manner, respectful of national sover eignty' (UNFCCC, 2016).

The Paris Agreement was officially available for signature on the 22nd of April 2016 at a signatory ceremony held in New York. As of 29 April 2016, there were 177 signatories to the Paris Agreement. Of these, 16 states have additionally deposited their instruments of ratification, acceptance or approval, in total accounting for 0.03 % of total global greenhouse gas emissions (UNFCCC, 2016).

2.1.2 National registries and emissions reporting

Globally binding emissions reductions targets provide a strong incentive for legislators to attain high resolution CO_2 emissions inventories to link emissions to particular regions and nations. Signatory parties are required to keep a national registry and report emissions to the UNFCCC. Current quantification methods estimate greenhouse gas emissions using economic emissions inventories, which rely on a 'bottom up' a pproach of reporting (as outlined by the IPCC Guidelines for National Greenhouse Gas Inventories; IPCC, 2006). The approximate carbon content of each fuel type is known, thus if the consumption data is known from economic data, the CO_2 emissions can be calculated. This technique of emissions quantification has an uncertainty of 10-15% at the national, annual scale (Marland et al., 2003), excluding any potential biases due to reporting errors.

In accordance with guidelines defined by the UNFCCC (and previously, the Kyoto Protocol), the New Zealand Government has committed to submit an official greenhouse gas inventory 15 months after the end of every calendar year. The most recent of which was released in April of 2015: New Zealand's G reenhouse Gas Inventory 1990-2013 (Ministry for the Environment, 2015). The data included in the report is a calculation of human-induced emissions that are categorised into 5 sectors: Energy (transport, electricity production), industrial processes and product use (metals, minerals and chemicals), agriculture (methane from livestock digestion, agricultural soils and manure management), LULUCF (land use, land use change and forestry) and waste (Figure 2.1).

Emissions described in the inventory are an aggregate of all anthropogenic GHGs, and are reported in carbon dioxide equivalent (CO_2-e) as a measure to describe the radiative forcing a given type and amount of a GHG may have, using the equivalent amount of CO_2 as a reference for consistency. The inventory does not outlined the contribution to total emissions by fossil fuel combustion alone,

which are contributed via a combination of transport (diesel, petrol and liquefied petroleum gas) and energy production (coal and natural gas).

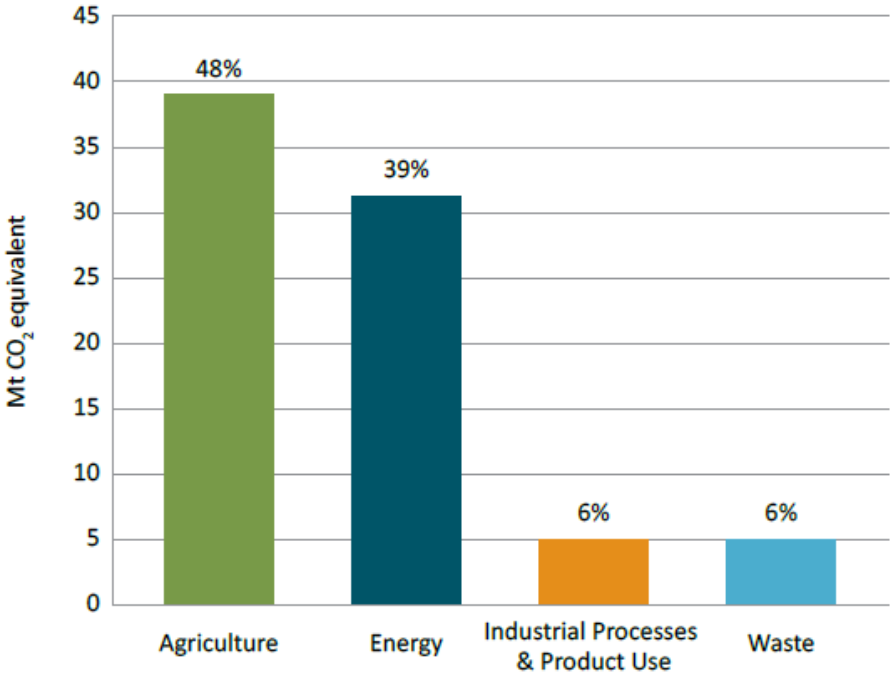

Figure 2.1: The 2013 New Zealand greenhouse gas emissions inventory (by sector, in million tonnes of CO_2-e), excluding LULUCF. Percentages do not equal 100 because of rounding (Ministry for the Environment, 2015).

The Ministry for the Environment is New Zealand's 'Inventory Agency' and the only assigned national entity for the greenhouse gas inventory. As the Inventory Agency, it is responsible for producing and submitting the greenhouse gas inventory to the UNFCCC (Ministry for the Environment, 2015). Inventory data is compiled in collaboration amongst the Ministry for the Environment, the Ministry of Business, Innovation and Employment, the Ministry for Primary Industries, and the Environmental Protection Authority. Additionally, much of the data is derived from data collated by Statistics New Zealand. As reported by the Ministry for the Environment, the uncertainty in net emissions (including the LULUCF) was ±11.2% for 2013. Uncertainty in the trend in net emissions since 1990 is ±12.3% (Ministry for the Environment, 2015).

The New Zealand national GHG inventory data does not provide information on emissions at the local level and is thus not useful for local governments. In New Zealand, it is not a legal requirement for local governments to provide an individual emissions inventory report. However, some regional councils, such as the Greater Wellington Regional Council, are taking it upon themselves to commission their own inventories to help inform their policies that address emissions reductions.

2.1.3 Local-scale attempts to address emissions

Cities are responsible for more than 70% of global energy-related CO_2 emissions (Gurney et al., 2015; Seto et al., 2012). Additionally, given the negligible progress made by national governmental bodies in response to international treaty negotiations pre-Paris Agreement, many cities all over the world began taking steps to independently address climate change and instigate emissions reduction schemes (Hoornweg et al., 2010).

To assist cities in developing standards and tools to measure their emissions, the World Resources Institute (WRI) and the World Business Council for Sustainable Development (WBCSD) developed the Greenhouse Gas Protocol (GPC; GHG Protocol, 2016). It serves as the foundation for nearly every GHG standard and program in the world, as well as hundreds of GHG inventories prepared by individual companies and now, some cities. The GPC works alongside the governing bodies of cities providing the standards and tools required to quantify local emissions, develop more effective emissions reduction strategies, set measurable and more ambitious emissions reduction goals, and to accurately track reductions progress (GHG Protocol, 2016).

In general, the calculation methodologies used by the GPC is in adherence to the IPCC Guidelines for National Greenhouse Gas Inventories (IPCC, 2006). For some activities, direct measurements of GHG emissions can be used, for example: emissions monitoring systems at power stations. However, for the majority of emissions sources, GHG emissions will need to be estimate, which is achieved by multiplying activity data by an emission factor associated with the activity being measured (GHG Protocol, 2016). The GHG Protocol defines activity data as a 'quantitative measure of a level of activity that results in GHG emissions taking place during a given period of time', such as volume of gas used or kilometres driven etc. An emission factor is a 'measure of the mass of GHG emissions relative to a unit of activity'.

It is not standard protocol for the GPC to verify inventory results; however it does recommend that governmental bodies to choose a level and style of verification that fulfils their individual needs. Verification involves an assessment of the accuracy of reported data. Cities may choose to verify data in order to demonstrate that emissions calculations are in agreement with the requirements of the GPC and ensure reported GHG emissions are a reasonable reflection of a city's activities. Verification can be performed by self-verification, where the same organisation that conducted the GPC assessment conducts the verification process, or by third-party verification, by an independent organisation (GHG Protocol, 2016).

As part of the 2014 Climate Change Strategy report, the Greater Wellington Regional Council (GWRC) demonstrated a commitment to reducing GHG emissions across all its areas of influence, including its own operations helping to create the conditions for a "smart innovative low carbon regional economy". A Wellington Region GHG Inventory was published by URS NZ Ltd, which was commissioned by five councils in the region to illustrate an emissions breakdown by district for the financial years 2000/2001 – 2012/2013 and produce emissions projection scenarios (GWRC, 2014; Figure 2.2).

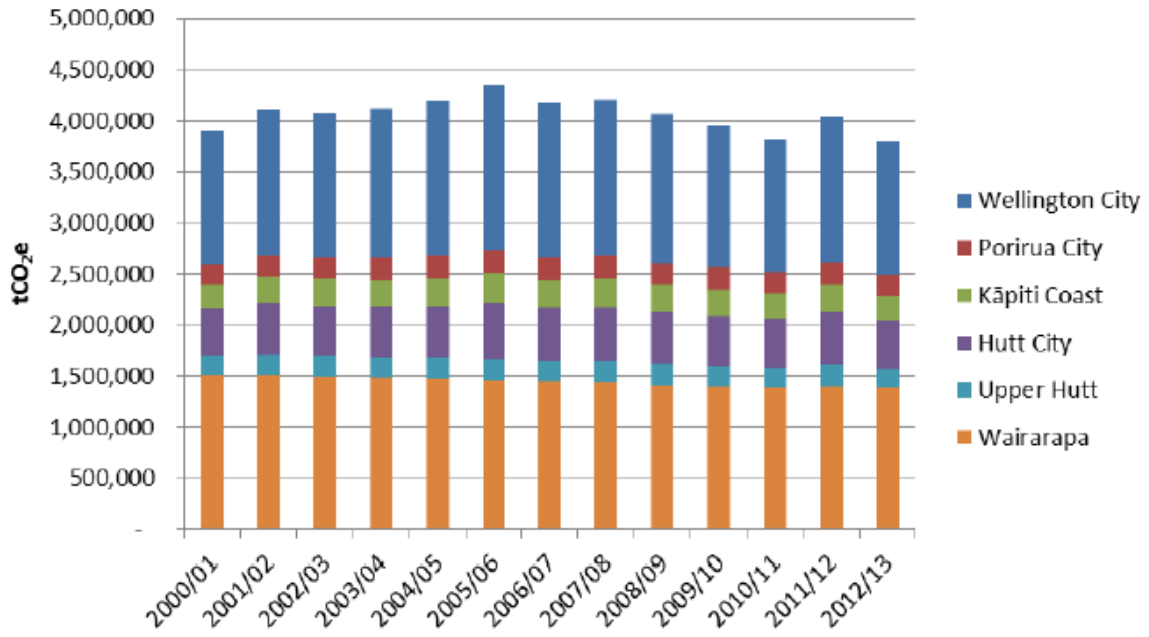

Figure 2.2: Wellington Region gross emissions profile (excluding LULUCF) per city and districts.

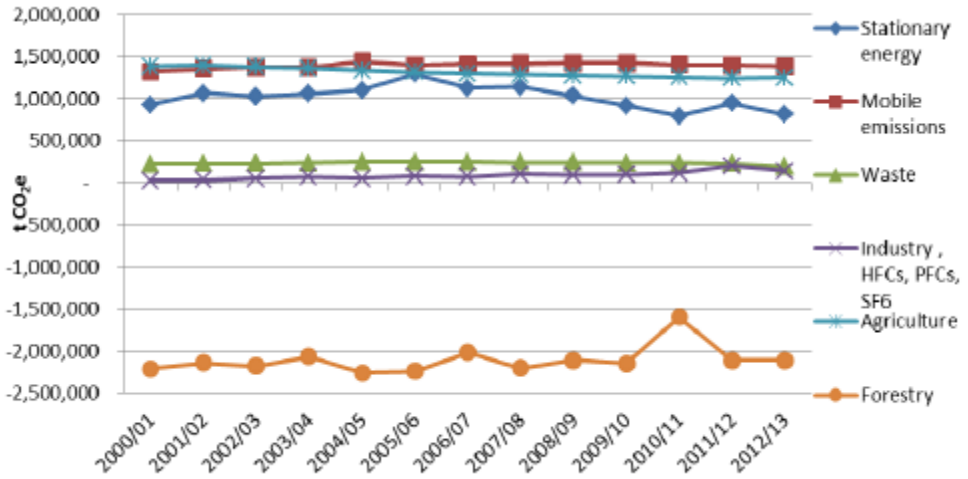

Figure 2.3: Regional net emissions profile (including LULUCF) by emissions source.

The Wellington Region GHG Inventory cannot be compared to the national level inventory on either an absolute or a per capita basis due to differing methodologies, regional scope and various assumptions; however there is some value in comparing relative emissions profiles and trends. The Wellington Region GHG Inventory breaks down emissions sources to a more detailed level, defining six emissions sources: Stationary energy, mobile emissions, waste, industry, agriculture and forestry (Figure 2.3). The inventory data has defined the fuel contribution (equivalent to the CO_{2ff} contribution) to total emissions to be relatively stable from 2001 to 2013 at approximately 280,000 tCO_2-e (GWRC, 2014). This inventory did not employ a standardised verification technique to validate the emissions estimates.

City-scale emissions inventories are important for local municipalities, such as the GWRC, to set emissions reduction targets. However, due to large uncertainties most cities lack independent, comprehensive and comparable sources of data (Marland et al., 2009). It is important that emissions inventories are grounded with scientific research that includes an understanding of the magnitude and mechanisms of CO_2 exchange between sources and the atmosphere to verify inventories based on emissions estimates. Thus, studies that match sources of CO_2 with atmospheric concentrations could help policy bodies to develop improved climate and emissions reduction policies.

2.1.4 International examples of emissions verification

'Bottom-up' approaches to emissions reporting have large uncertainties due to temporal extrapolation of trends and spatial redistribution of inventory-based emissions according to population density (Marland et al., 2009; Nisbet & Weiss, 2010). Additionally, there is currently no standardised method to verify reported emissions (as well as reductions) using actual variations in emissions from direct atmospheric measurements. However, there are some local governing bodies that are developing top-down atmospheric measurements that are reported to the UNFCCC.

Since 2012, the Australian Government in conjunction with the Commonwealth Scientific and Industrial Research Organisation (CSIRO) have been performing atmospheric measurements of GHGs that are ozone depleting substances (ODSs) to comply with the Montreal Protocol (1987) and are reported along with the Australian GHG inventory to the UNFCCC (Fraser et al., 2013). These include: chlorofluorocarbons (CFCs), hydrochlorofluorocarbons (HCFCs), halons, carbon tetrachloride (CTC: $CCl_{4)}$, methyl chloroform (MC: $CH_3CCl_{3)}$, and methyl bromide (MB: CH_3Br).

Despite that the majority of these substances are no longer imported or produced in Australia, atmospheric observations completed at Cape Grim, Tasmania show there are measurable emissions of these chemicals from Melbourne and Port Phillip area (Montzka and Reimann, 2011). These

remnant emissions are most likely from ‘banks’ of these species, such as ODS containing equipment 9still in use or contained in landfills: refrigerators, aerosol cans, fire extinguishers and foam plastics (Fraser et al., 2012). Atmospheric measurements of this kind are vital in order to detect sources of ODSs, which exist despite no longer being in use within Australia.

As party to the UNFCCC and Kyoto protocol, EU monitoring mechanism regulation and the UK Climate Change Act (2008), the United Kingdom was committed to reducing GHGs and, like New Zealand, was required to submit a national emissions inventory. The inventory is based on range of sources, including reporting by the UK government, other governmental bodies and industry. On top of inventory data, the Department of Energy and Climate Change (DECC) monitors concentrations of atmospheric gases in order to ascertain a state of the atmosphere, to inform policies to reduce emissions of pollutants and verify the UK GHG inventory (DECC, 2013).

The DECC, in collaboration with the University of Bristol, maintains a research programme that makes high-frequency, high-precision measurements of atmospheric gas concentrations at the Mace Head Research Station on the West coast of Ireland. Mace Head monitors clean well-mixed westerly air as it travels across North Atlantic Ocean, which allows estimates of Northern Hemisphere baseline concentrations of gases to be made (DECC, 2013). When there is an easterly at Mace, regional-scale pollution in air that has travelled from industrial regions of Europe is measured. Comparing these two data sets, gas concentrations contributed by humans can be determined using a modelling technique used specifically for the DECC research programme, InTEM (Inversion Technique for Emission Modelling). This work is carried out for DECC by the Met Office, and uses the Met Office NAME (Numerical Atmospheric dispersion Modelling Environment) model to understand the recent history of air arriving at Mace Head (DECC, 2013).

Neither the GHG Inventory estimates, nor the InTEM atmospheric measurements, provides absolutely certain UK emissions values. Uncertainty in the inventory and InTEM estimates (including analytical and modelling components) vary by gas, thus are reported alongside the emissions estimates on a gas-by-gas basis. Comparing the Inventory and InTEM estimates for the key GHGs, there is good agreement for nitrous oxide. Methane estimates are consistently lower in InTEM than in the inventory in the 1990s, but post-2000 they do agree, within the uncertainty. Verification of CO_2 emissions is more difficult because natural sources of CO_2 are significant and emissions vary strongly in time, therefore these results are unreliable and have not yet been used to verify the inventory with confidence (DECC, 2013). Alternatively, the radiocarbon method is a technique that can distinguish between fossil and non-fossil sources of CO_2 that can be employed as an unambiguous tracer for fossil fuel CO_2 emissions (Turnbull et al., 2011a).

2.2 Radiocarbon in the carbon cycle

2.2.1 Introduction

To accurately measure the CO_2 concentration in the atmosphere and to determine the relative contribution by anthropogenic activities, an understanding of carbon cycling is needed. It is known that there has been an unprecedented increase in CO_2 concentration in the atmosphere, increasing from pre-industrial levels of 290 ppm to current values of ~400 ppm (Tans & Keeling, 2016). Recent estimates of the CO_2 contribution attributed to fossil fuels is 9.8 gigtons of carbon (GtC) per year (as at 2013; Boden et al., 2015). The rate of increase in the atmospheric CO_2 burden of 3.09 ppm per year (as at 2015; Dlugokencky & Tans, 2016) demonstrates that only just over half of the CO_2 emitted as a result of human activity (CO_{2ff}) persists in the atmosphere (Dlugokencky & Tans, 2016). The remainder is absorbed by other Earth reservoirs: the oceans and terrestrial biosphere.

Carbon cycle models suggest that uptake of anthropogenic CO_2 between the oceans and biosphere is roughly evenly distributed (Cias et al., 2013); however this process of apportionment is not perfectly understood. Uptake is affected by interannual variability, which is largely attributed to variability in the terrestrial biospheric carbon flux. This is likely due to climate variability, but mechanisms of exchange processes still remain poorly understood. Additionally, it is difficult to separate the biospheric exchange flux from CO_{2ff} as the two carbon sources are co-located at the surface over continental (largely Northern Hemispheric) land. An improved understanding of the magnitude and mechanisms of carbon exchange with the biosphere is needed to accurately predict the rate of atmospheric CO_2 change over time. Measuring the radiocarbon (^{14}C) content of CO_2 is a commonly used method to accurately differentiate CO_{2ff} from biosphere contributions. Here we explore the complex carbon cycle and explain in accompanying equations, the role of ^{14}C and how it can be applied to emissions quantification.

2.2.2 The global carbon cycle

The global carbon cycle describes the exchange of carbon between the Earth's c arbon reservoirs and the atmosphere (Ciais et al., 2013; Figure 2.4), which can be distinguished into two domains, the 'fast domain' or the 'slow domain'. The *fast domain* defines large exchange fluxes and relatively rapid reservoir turnovers that range from a few years to millenia. This determines carbon exchange between the atmosphere, ocean and on land (vegetation, soils and freshwaters). The *slow domain* exchanges at a slower rate, in the order of 10,000+ years. This includes carbon stores in rocks and sediments that exchange carbon with the fast domain through volcanic emissions of CO_2, erosion and sediment formation on the sea floor (Sundquist, 1986).

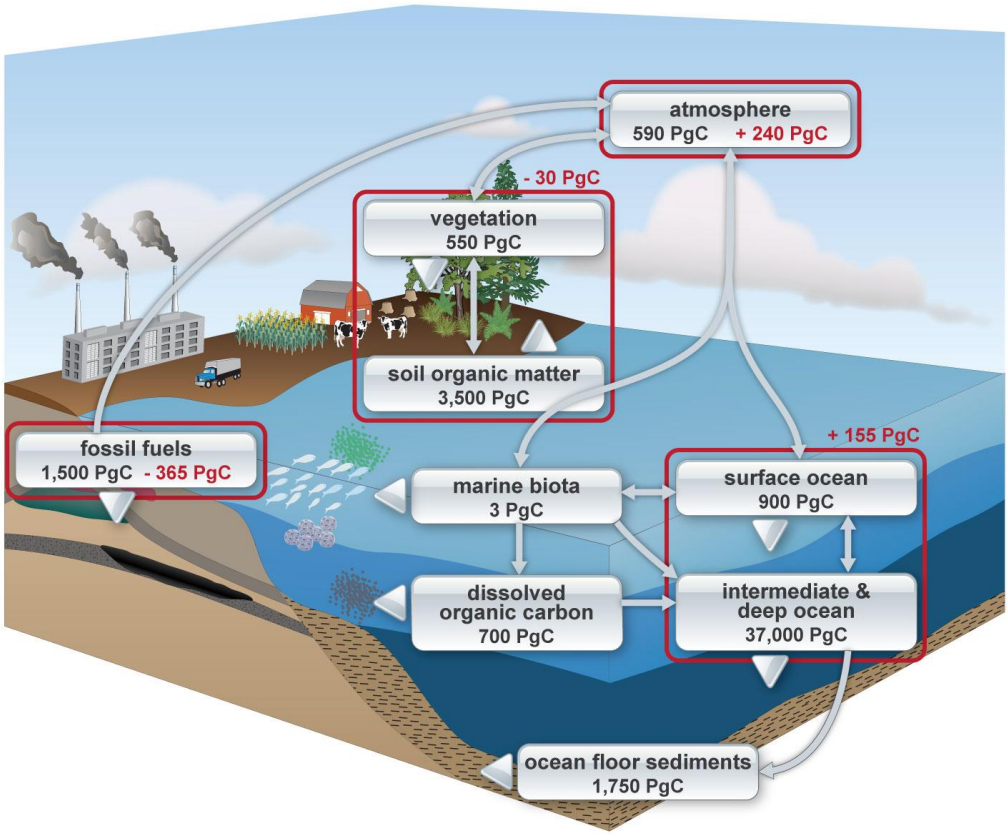

Figure 2.4: The global carbon cycle (Schuur et al., 2016), using numbers published in Fig 6.1 of IPCC (2013). This diagram shows natural fluxes from the ocean, atmosphere and terrestrial biosphere and the contribution of anthropogenic perturbations (fossil fuels).

Prior to the industrial revolution (1750 AD), the fast domain was close to a steady state, as seen from relatively small variations in CO_2 measured in ice cores (Elsig et al., 2009). Since the beginning of the Industrial Era, fossil fuel extraction from geological reservoirs and their subsequent combustion have resulted in the rapid transfer of a significant amount of fossil carbon from the slow domain into the fast domain – thus causing an unprecedented, human-induced perturbation of the carbon cycle (Ciais et al., 2013).

As well as a dynamic global cycle, CO_2 has a seasonal and diurnal cycle influenced by the process of carbon uptake by vegetation during photosynthesis and respiration from biosphere (vegetation, animals and soils). This seasonal oscillation reflects uptake of CO_2 by vegetation during daylight hours in the 'growing season' - the timing of which is keyed to the Northern Hemisphere seasons due to the Northern Hemisphere's abundance of continental land, which contains the majority of Earth's terrestrial biosphere. This cycle is reversed in autumnal periods when photosynthesis slows and respiration (release of CO_2) by heterotrophic and autotrophic organisms is dominant.

Atmospheric CO_2 concentration also varies strongly regionally, due to relative distance from carbon sources and sinks. In the Northern Hemisphere - where there is abundant vegetation - there is a strong exchange flux of carbon between terrestrial biosphere and the atmosphere. Additionally, the majority of fossil fuel emissions are emitted in the Northern Hemisphere, creating plumes of CO_2 that are transported via air masses. In the Southern Hemisphere - where there is a lack of continental land and instead, a vast expanse of water - the largest influence on atmospheric CO_2 is ocean exchange (Siegenthaler & Sarmiento, 1993). Carbon uptake and release occurs in oceans via gas exchange between the atmosphere and surface waters. The ocean acts as a carbon sink when upwelling water is deplete in dissolved CO_2. The ocean acts as a carbon source when upwelling water is CO_2-replete and CO_2 is consequently released to the atmosphere. Multiple factors impact the rate of exchange and the gross one-way fluxes into and out of the ocean, which are about 80 Pg C year $^{-1}$, however, on an annual to decadal timescale, the net ocean flux is approximately neutral (Schuur et al., 2016).

2.2.3 The global carbon dioxide budget and $^{14}CO_2$

The atmospheric CO_2 budget can be described by the following equation:

$$\frac{dC_a}{dt} = F_p + F_r + F_{ao} + F_{oa} + F_{ff} \quad (2.1)$$

Where:

C_a = atmospheric CO_2

F_p and F_r = CO_2 fluxes into and out of the terrestrial biosphere

F_{ao} and F_{oa} = the fluxes from the atmosphere into the ocean and vice versus

F_{ff} = the flux into the atmosphere from fossil fuel emissions

In this notation, fluxes into the atmosphere (F_r, F_{oa}, F_{ff}) are all positive, and fluxes out of the atmosphere (F_p, F_{ao}) are negative. For continental measurements the effects from ocean ($F_{oa,}$ F_{ao}) can be excluded (Schuur et al., 2016).

There are three naturally occurring carbon isotopes, two of which are stable, ^{12}C (98.89%) and ^{13}C (1.11%), and one that is unstable, ^{14}C (<0.1%). ^{14}C is produced naturally in the atmosphere as a result of the interaction between cosmic ray-induced neutrons and nitrogen (^{14}N). The ^{14}C produced reacts to form ^{14}CO and $^{14}CO_2$, before exchanging into Earth's carbon reservoirs, where radioactive decay decreases the ^{14}C concentration.

The half-life of ^{14}C is 5730 ± 40 years (Godwin, 1962), thus *fast domain* carbon reservoirs that exchange relatively rapidly with the atmosphere have a ^{14}C content close to that of the atmosphere. Whereas *slow domain* reservoirs, cut off from the atmosphere (e.g. fossil fuel reservoirs below the Earth's surface) for a period longer than about ten half-lives, are devoid of ^{14}C.

^{14}C has a short residence time in the terrestrial biosphere, in the order of 10-20 years (Trumbore, 1997). Current CO_2 flux entering the atmosphere via respiration from the terrestrial biosphere reflects an atmospheric $\Delta^{14}C$ signal from ~10 years ago (Turnbull, 2006a). Most radioactive decay of ^{14}C occurs in the ocean reservoir and the $\Delta^{14}C$ of subsurface waters is dominated by radioactive decay in the time since last contact with the atmosphere. Mean subsurface residence time before returning to the surface is on the order of a thousand years, producing surface ocean $\Delta^{14}C$ values significantly lower than the atmosphere (Turnbull, 2006a).

There are four main factors driving isotopic differences in $\Delta^{14}C$ between carbon sources and the atmosphere disequilibrium in ^{14}C between the sources and the atmosphere (Turnbull, 2006a):

i. Natural production of ^{14}C by the interaction of nitrogen with cosmic rays in the upper atmosphere
ii. The reservoir age that determines the ^{14}C content in each carbon reservoir/source
iii. Anthropogenic production of ^{14}C from nuclear weapons testing and the nuclear industry
iv. Fossil fuel emissions

Changes in ^{14}C can be described by the following equation:

$$\frac{dC_a\Delta_a}{dt} = F_p\Delta_p + F_r\Delta_r + F_{ao}\Delta_{ao} + F_{oa}\Delta_{oa} + F_{ff}\Delta_{ff} + F_c\Delta_c + F_n\Delta_n + F_d\Delta_d \quad (2.2)$$

Where:

Δ = ^{14}C value of the denoted pool of flux (Tans et al., 1979).

F_c = the flux due to natural cosmogenic production of ^{14}C in the stratosphere

F_n = the flux due to anthropogenic activities, namely nuclear weapons testing and the nuclear power industry

F_d = the negative flux due to radioactive decay, which is too small to influence decadal to century-scale changes in atmospheric ^{14}C and is therefore ignored hereafter

The three new terms in the ^{14}C budget (F_c, F_n, and F_d) are all pure ^{14}C fluxes, that despite being very small, have a large impact on $^{14}CO_2$. This equation describes the entire atmosphere as a single pool,

but as the stratosphere is the primary site of cosmogenic production, is enriched in ^{14}C relative to the troposphere, it can be treated as a separate pool (Levin et al., 2010).

Combining the first two equations we obtain:

$$C_a \frac{d\Delta_a}{dt} = F_r(\Delta_r - \Delta_a) + F_{oa}(\Delta_{oa} - \Delta_a) + F_{ff}(\Delta_{ff} - \Delta_a) + F_c(\Delta_c - \Delta_a) + F_n(\Delta_n - \Delta_a) + F_p(\Delta_p - \Delta_a) + F_{ao}(\Delta_{ao} - \Delta_a)$$

(2.3)

Each term on the right hand side of the equation represent the isofluxes of the four factors that drive isotopic differences in ^{14}C: cosmogenic production, carbon reservoir age (of the ocean and terrestrial biosphere), anthropogenic nuclear activities and fossil fuel emissions. Isofluxes are the product of one-way gross CO_2 flux and the isotopic difference between the source (or sink) and the atmosphere, otherwise known as isotopic disequillibrium.

A relatively small CO_2 flux can have a large isoflux should the isotopic disequilibrium between the atmosphere and a particular reservoir is large. Conversely, a large CO_2 flux can have small or zero isoflux if there is little or no isotopic disequilibrium between the atmosphere and the reservoir.

Isofluxes may be positive or negative, depending on the sign of the isotopic disequilibrium and the isoflux may be of a different sign than the CO_2 flux. When carbon is dissolved into the surface ocean or taken up by plants (fixed by photosynthesis) the only change in isotopic composition is due to mass-dependant fractionation during the uptake, which is corrected for in the ^{14}C nomenclature. Therefore, p, and ao, are by definition equal to a, so the isotopic disequilibrium in uptake is zero. As a result the last two terms in equation 3 that represent the isofluxes into the biosphere and oceans are equal to zero.

Thus:

$$C_a \frac{d\Delta_a}{dt} = F_r(\Delta_r - \Delta_a) + F_{oa}(\Delta_{oa} - \Delta_a) + F_{ff}(\Delta_{ff} - \Delta_a) + F_c(\Delta_c - \Delta_a) + F_n(\Delta_n - \Delta_a)$$

(2.4)

The remaining terms in the last equation are all fluxes of CO_2 into the atmosphere. Therefore, measurements of ^{14}C of CO_2 ($\Delta^{14}CO_2$) detect the one-way gross fluxes into the atmosphere, rather than the net fluxes that are detected by CO_2 concentration measurements. Understanding the movement of CO_2 through carbon sources and sinks is in important in order to interpret atmospheric observations of $^{14}CO_2$ and thus anthropogenic additions of CO_2.

2.3 Historic timeline of radiocarbon distribution

2.3.1 Preindustrial distribution of radiocarbon

Prior to 1850, the fossil fuel and nuclear isofluxes were negligible, thus only cosmogenic production, radioactive decay and land and ocean exchanges influenced atmospheric $^{14}CO_2$ (Schuur et al., 2016). Cosmogenic production was the only positive isoflux, which contributed to an increase of approximately 9 ‰ year $^{-1}$ (Schuur et al., 2016). Both terrestrial biosphere and oceans contributed a negative isoflux, as carbon resides in each of these reservoirs for an extended period of time, therefore becoming depleted in ^{14}C due to radioactive decay before being cycled back into the atmosphere. As the biospheric residence time is typically shorter than that of the oceans, the ocean isoflux was the dominant influence on $^{14}CO_2$ (versus the land isoflux) in the preindustrial atmosphere (Schuur et al., 2016).

2.3.2 The Suess Period; 1890-1945

The first observation of anthropogenic influence on atmospheric $^{14}CO_2$ was made by Suess (1955), which showed a decrease in $^{14}CO_2$ in the early part of the 1900s in tree-ring records from North America, a phenomenon referred to as the *Suess Effect*. This decline in atmospheric $^{14}CO_2$ is attributed to the addition of ^{14}C-depleted fossil fuel CO_2 to the atmosphere since the industrial revolution (Schuur et al., 2016). Suess' tree-ring measurements showed a decrease of 25‰ in atmospheric $\Delta^{14}CO_2$ between 1890 and 1950 (Suess 1955). This observed decline in $^{14}CO_2$ was not determined exclusively by an increased rate of fossil fuel emissions. Gross exchanges of carbon between the atmosphere and Earth's surface reservoirs moderate $^{14}CO_2$-dilution by effectively increasing the reservoir of carbon into which the ^{14}C-depleted fossil fuel CO_2 is mixed. Some fossil-derived carbon enters the Earth's surface reservoirs via gross exchanges and is ultimately replaced in the atmosphere by carbon that has the ^{14}C signature of the oceanic and terrestrial biosphere (Schuur et al., 2016).

2.3.3 The "bomb period"; 1945-1985

Up until the mid-20th century the addition of fossil fuel-derived emissions was relatively small, thus the ^{14}C signature of the atmosphere was relatively stable. However, atmospheric nuclear weapon testing in the 1950s and 60s released a large amount of ^{14}C into the atmosphere, almost doubling the atmospheric ^{14}C concentration (Figure 2.5). This large pulse of ^{14}C quickly oxidised to $^{14}CO_2$ and subsequently entered the carbon cycle and was absorbed by oceans and assimilated by plants. Peak concentration of ^{14}C (the 'bomb spike') was reached in the Northern Hemisphere in 1963 and in the

Southern Hemisphere by 1965, and has rapidly declined since the instigation of the International Test Ban Treaty in 1963 (Nydal, 1968; Levin et al., 1985, Currie et al., 2011).

The 'bomb spike' provides a useful time stamp and the excess ^{14}C has been used as a CO_2 tracer. Bomb radiocarbon has therefore made a major contribution to carbon cycle research, such as: atmospheric transport, ocean circulation and carbon flux, CO_2 exchange between reservoirs and turnover time in terrestrial biosphere (Broecker et al., 1995; Levin et al., 2010).

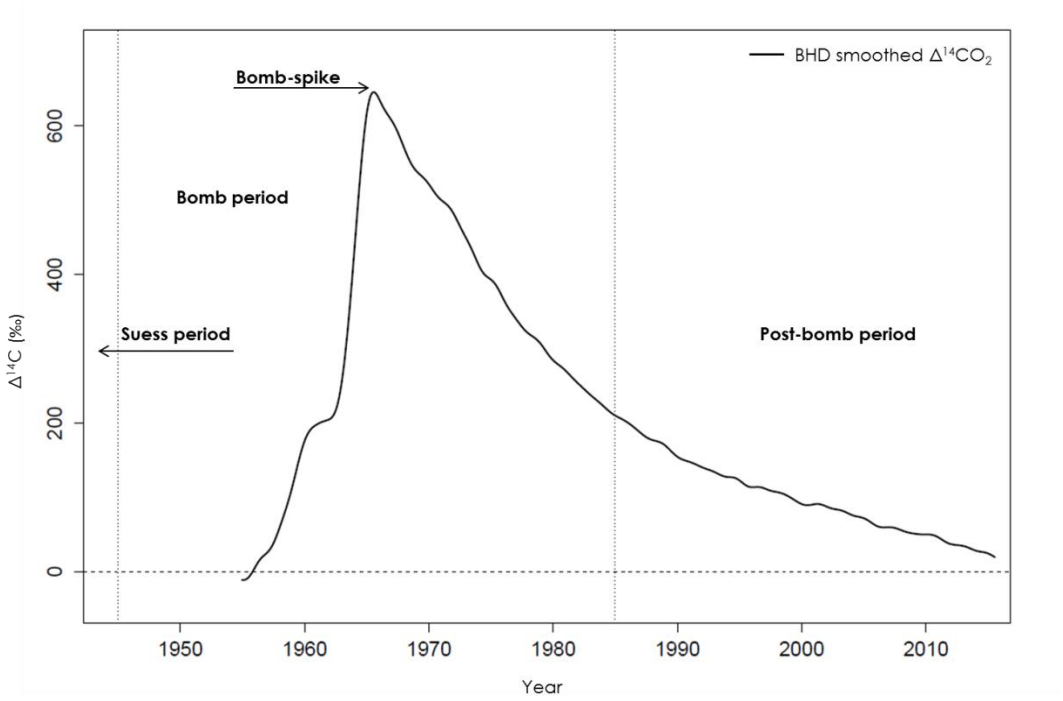

Figure 2.5: Observations of $\Delta^{14}CO_2$ measured from Baring Head (Turnbull et al., 2014a).

2.3.4 The post-bomb period; 1985-present

More recently, bomb ^{14}C has almost reached equilibrium in the atmosphere (Figure 2.5). This is in part due to rapid uptake of the bomb ^{14}C by surface reservoirs contributing to a decrease in the tropospheric $^{14}CO_2$ content and simultaneous increase in ^{14}C in the surface reservoirs. The persistent increase in the production of fossil fuel-derived CO_2 emissions has also contributed to the change in atmospheric $^{14}CO_2$ signal. Since the mid-1980s several atmospheric CO_2 studies determine a change in prevalence of the biosphere CO_2 contribution, which coincides with a change to fossil fuel CO_2 becoming the dominant driver of variability in $^{14}CO_2$ (Randerson et al., 2002; Levin et al., 2010).

Fossil fuel-derived CO_2 emissions have grown substantially over the post-bomb period, approximately doubling between 1980 and 2012 (Boden et al., 2012). Dilution of $^{14}CO_2$ by fossil-derived CO_2 is now the greatest contribution to the long-term trend and inter-hemispheric gradient of $^{14}CO_2$ in unpolluted background air (Figure 2.5; Randerson et al., 2002; Turnbull et al., 2009).

2.4 Atmospheric monitoring of fossil fuel emissions

2.4.1 The Baring Head Clean Air $^{14}CO_2$ Record

The history of atmospheric $^{14}CO_2$ through the post-bomb period has been directly measured at several 'clean air' sites around the world, one of which is located at Baring Head, in New Zealand, atop a sea cliff on the eastern side of the Wellington Harbour entrance (Figure 2.6). Observations of atmospheric CO_2 have taken place at this site since the early 1970s. Combined with the preceding measurements made at a site in Makara (New Zealand; established in 1954), these measurements construct the longest record of tropospheric $\Delta^{14}CO_2$ in the world (Currie et al., 2011, Turnbull et al., 2014a).

Figure 2.6: Location map of two atmospheric clean air monitoring sites in the Wellington Region, New Zealand.

The $\Delta^{14}CO_2$ data is collated by samples collected over a typically two-week period at monthly intervals by static absorption into a carbonate-free NaOH solution. CO_2 is extracted from the NaOH solution by acidification followed by cryogenically trapping (Rafter & Fergusson, 1959). Up until 1995 the ^{14}C content of CO_2 was determined by a proportional gas-counting technique. Currently, $^{14}C/^{12}C$ ratio measurements are performed by accelerator mass spectrometry (AMS) at the Rafter Radiocarbon Laboratory, GNS Science. The dataset has recently been revised and there have been updates to the data, particularly in areas that previously had large uncertainty, with higher precision AMS measurements (Turnbull et al., 2014a; Turnbull et al., 2015).

The Baring Head atmospheric ^{14}C time-series over the past 60 years is dominated by the bomb spike of the mid 1960s, occurring about two years later than seen in records from the Northern Hemisphere (as the vast majority of detonations took place in the Northern Hemisphere). Post-1965, transfer of ^{14}C-enriched CO_2 occurred between the atmosphere and the biosphere and oceanic sinks resulted in a decrease of atmospheric ^{14}C. Additionally, the on-going release of ^{14}C-depleted CO_2 from fossil fuel combustion contributes to this observed decrease, particularly in the last 30 years.

2.4.2 Determination of fossil fuel mole fraction from radiocarbon observations

This fossil fuel 'signature' in the atmosphere can be distinguished from other sources of CO_2 that contain ^{14}C levels close to that of the atmospheric background (Suess, 1955; Levin et al., 2003; Turnbull et al., 2009). Therefore, it is possible to discern the anthropogenic contribution to the atmospheric CO_2 concentration by measurement of the ^{14}C content of CO_2, expressed as $\Delta^{14}CO_2$ (Levin et al., 2003; Turnbull et al., 2006b).

Atmospheric $\Delta^{14}CO_2$ measurements have been recognised as an unambiguous tracer method to quantify fossil fuel CO_2 (CO_{2ff}) emissions, thus providing an objective method of evaluating CO_{2ff} emissions reported by governments and industry. Additionally, the separation of fossil fuel and biological CO_2 sources by $^{14}CO_2$ allows the examination of biological CO_2 exchange processes.

A mass balance equation (an integration of Equation 4.1 and 4.2) is used to calculate the fossil fuel CO_2 contribution in an atmospheric sample for which $\Delta^{14}CO_2$ has been measured:

$$CO_{2obs} = CO_{2bg} + CO_{2ff} + CO_{2other} \quad (2.5)$$

and:

$$\Delta_{obs}CO_{2obs} = \Delta_{bg}CO_{2bg} + \Delta_{ff}CO_{2ff} + \Delta_{other}CO_{2other} \quad (2.6)$$

Then manipulated to solve for CO_{2ff}:

$$CO_{2ff} = \frac{CO_{2obs}(\Delta_{obs} - \Delta_{bg})}{\Delta_{ff} - \Delta_{bg}} - \frac{CO_{2other}(\Delta_{other} - \Delta_{bg})}{\Delta_{ff} - \Delta_{bg}} \quad (2.7)$$

Where:

CO_{2other} = all non-fossil influences on $^{14}CO_2$ that add of remove CO_2 (respiration and biomass burning, nuclear industry, oceans and cosmogenic production)

Δ_{other} = flux weighted average of Δ values for all other sources/sinks

CO_{2bg} = background air CO_2 mixing ratio

Δ_{bg} = background air $\Delta^{14}CO_2$ value

To place emphasis on the influence fossil fuel combustion, all 'other' terms contributing to atmospheric CO_2 have been condensed into the single term: CO_{2other}, which is essentially a correction for all non-fossil influences on $^{14}CO_2$ (Schuur et al., 2016). The influence that different non-fossil source have on the CO_{2ff} signal is dependent on location and regional variables. For example, cosmogenic production does not have a strong influence as it occurs high in the atmosphere and does not change the spatial distribution of CO_2 at the Earth's surface (Turnbull et al., 2009; Levin et al., 2010). Furthermore, ^{14}C from nuclear power sources is negligible in the Southern Hemisphere as almost all nuclear emissions occur in the Northern Hemisphere (Hesshaimer et al., 1994). At coastal or marine sites, ocean exchange presents a potential bias. This is most prevalent in areas near upwelling regions in the Southern Ocean or Pacific Ocean where the isotopic disequilibrium between atmosphere and ocean is at its greatest (Randerson et al., 2002; Turnbull et al., 2009). This effect can be eliminated by an appropriate Δ_{bg} reference, for example, using measurements that reflect the same ocean influence as the region of interest (Schuur et al., 2016). ^{14}C of photosynthetic uptake is equal to Δ_{bg} and is therefore excluded, thus we can rewrite the equation to make (Turnbull et al., 2009):

$$CO_{2ff} = \frac{CO_{2bg}(\Delta_{obs} - \Delta_{bg})}{\Delta_{ff} - \Delta_{obs}} - \frac{CO_{2r}(\Delta_r - \Delta_{obs})}{\Delta_{ff} - \Delta_{obs}} \quad (2.8)$$

Conversely, $\Delta_r \neq \Delta_{bg}$ due to the disequilibrium problem; where CO_2 emitted via heterotrophic respiration has a $\Delta^{14}C$ value equivalent to that of the atmosphere at the time the CO_2 was photosynthesized, and atmospheric $\Delta^{14}C$ has rapidly changed through time. This is in contrast to autotrophic respiration, which returns carbon to the atmosphere rapidly and does not have the same disequilibrium effect as heterotrophic respiration. The contribution of Δ_r must be calculated as it varies between sites dependent on variable factors such as soil carbon residence time. For example, assuming a residence time of ~10 years for heterotrophic respired CO_2, Δ_r = 75 ‰ (45‰ higher than Δ_{bg}).

2.4.3 Fossil fuel CO_2 spatial variability and plant radiocarbon as a proxy

Global $^{14}CO_2$ modelling studies (Randerson et al., 2002; Turnbull et al., 2009) have been used to examine spatial variability of $^{14}CO_2$ in the recent atmosphere (Figure 2.7). These models represent the best estimates of ^{14}C isoflux magnitudes as well as spatial and temporal patterns. These global models have shown that $^{14}CO_2$ variability over the Northern Hemisphere land is dominated at the continental scale by CO_{2ff} emissions.

Plant materials have proven to be an excellent proxy for $^{14}CO_2$ at the continental, annual scale – allowing them to be used to understand the broad spatial distribution of $^{14}CO_2$ and to compare to model simulations (Hsueh et al., 2007; Riley et al., 2008; Bozhinova et al., 2013). Via photosynthesis, plant material faithfully records the ^{14}C content of local atmospheric CO_2, thus radiocarbon analysis of plant material provides an alternative sample collection method for $\Delta^{14}CO_2$ concentration. Plants assimilate CO_2 over a time interval that covers several weeks to months, and can reflect changes in atmospheric $^{14}CO_2$ signature (Bozhinova et al., 2013).

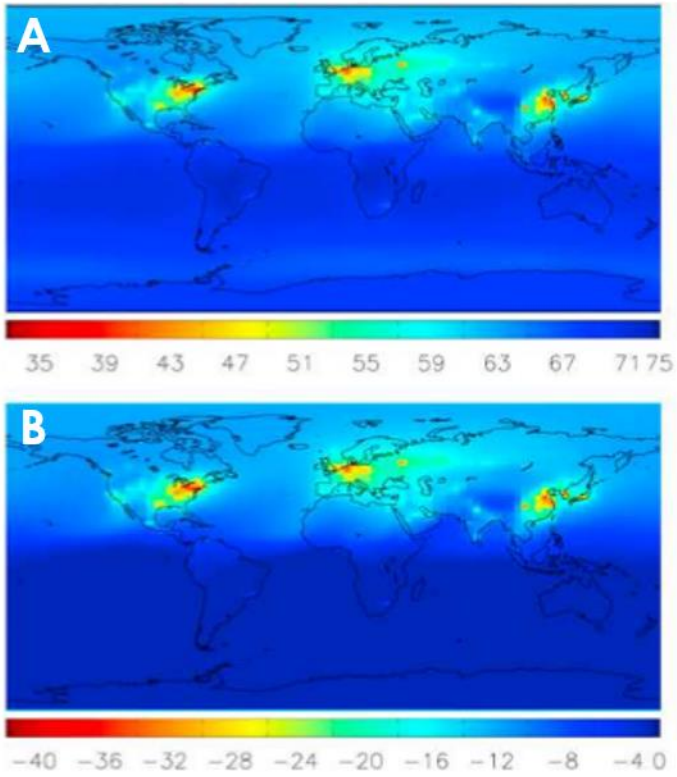

Figure 2.7: **A** - Modelled mean surface distribution of $\Delta^{14}CO_2$ for 2002–2007. **B** - Modelled surface distribution of $\Delta^{14}CO_2$ if fossil fuel CO_2 emissions were the only source of variability in $\Delta^{14}CO_2$; values are shown relative to the equator. Note that the scale range is identical (40‰) in both plots, and the surface level is taken as the lowest model level (Turnbull et al., 2009).

Using $\Delta^{14}CO_2$ measurements from tree rings is advantageous, rather than traditional collection methods such as air flasks, towers or NaOH samplers, as sampling can cover relatively long time periods, allowing retrospective records of atmospheric CO_2 to be constructed. However there are caveats, with photosynthetic uptake only in daylight periods $\Delta^{14}CO_2$ values are biased to daytime values and at an annual scale to the growing season (spring and summer; Hua & Barbetti 2004) and meteorological factors (Bozhinova et al., 2013).

Trees, particularly, show great potential for providing more long term records, with annual rings recording an annual record of $^{14}CO_2$. Tree rings have a long history of being utilised in palaeoclimate studies, particularly proxy studies of atmospheric conditions, climate, temperature and precipitation (Boswijk et al., 2014). A significant advantage of using tree rings is due to the annual formation of rings, thus allowing accurate chronologies to be developed. Tree rings have been used widely in radiocarbon studies to develop ^{14}C chronologies and create a radiocarbon calibration curve (Turney et al., 2007; Palmer et al., 2015, Reimer et. al., 2004). Previous studies have successfully used tree rings, in addition to direct atmospheric measurements, to measure global distribution of ^{14}C after the bomb spike in 1965 (Hua et al., 2000; Hua & Barbetti, 2013). Using^{14}C measurements of tree ring material have been used to monitor levels of anthropogenic emissions in urban landscapes. This is a developing research area, with studies being completed in various locations (Capano et al., 2010; Rakowski, 2011; Djuricin et al., 2012; Norris et al., 2015).

CHAPTER 3: METHODS

3.1 Study sites and sample collection

This study aims to demonstrate the utility of the radiocarbon method and explore the possible policy implications this method may have. Thus, executing field studies in a location where there is potential interest from local policy makers and urban planners is advantageous. For these reasons, Wellington is a good location to perform this study. In addition to this:

1. We have a strong understanding of urban development from the turn of the 20th century and access to detailed information pertaining to this;

2. There is good meteorological data available. The weather systems are well documented and the windy climate ensures the air is well-mixed.

3. Central Lower Hutt is a good place within the Wellington region to perform this study. It is accessible, has urban and coastal environments in relatively close proximity and has three trees of the appropriate species available for sampling.

Three trees from two different sites were chosen based on their age and species (Figure 3.8):

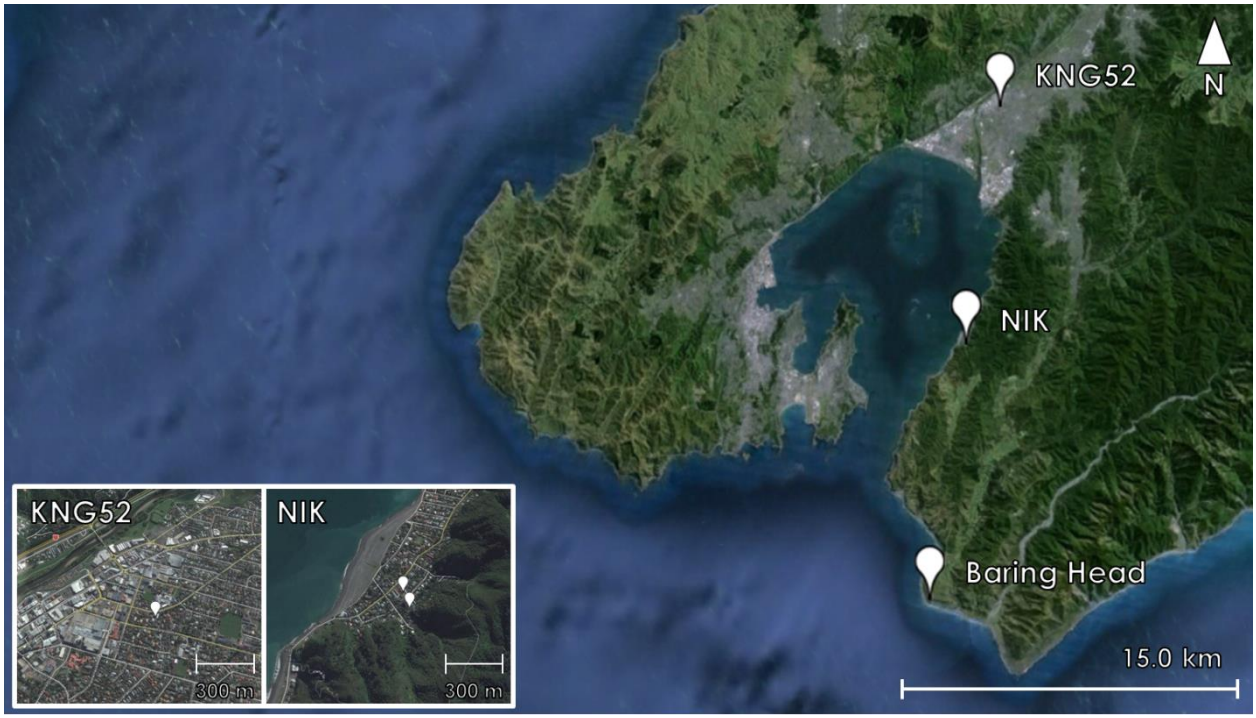

Figure 3.8: Sample site locations. KNG52: Test site, provides a 'polluted air' record due to its proximity to the urban environment; NIK: Tree core samples NIK19 and NIK23, provides a record representative of background $^{14}CO_2$

3.1.1 Background site: Nikau St, Eastbourne

Tree samples NIK19 and NIK23 (19, 23 Nikau Street, Eastbourne; Figure 3.9) will be used in combination for confirmation of the background CO_2 record for this study. These trees are two Kauri (*Agathis australis*), identified using the New Zealand Trees Register (New Zealand Notable Trees Trust, 2009).

Eastbourne is a residential village on the coast, population 5,000. Nikau Street is at the southern end of Eastbourne, 250m from the beach. There is light vehicle traffic associated with local residents and residential coal, gas and wood combustion for heating and cooking. Local knowledge suggests that these effects would contribute only small amounts of CO_{2ff} thus it is expected to provide a record representative of background (atmospheric) CO_2. Comparison with the Baring Head Clean Air record (measured at a station about 11.3km south of NIK site; Currie et al., 2011) will be used to confirm this (Chapter 4.1.1). Additionally, by comparing the NIK record to the already established Clean Air record, it will be determined whether tree ring ^{14}C directly reflects local atmosphere and if there are any unexpected variations in the data due to the use of plant assimilated ^{14}C to develop the record (Turnbull et al., 2014b).

Figure 3.9: Location of two background Kauri trees: NIK19, 19 Nikau Street, Eastbourne; NIK23, 23 Nikau Street, Eastbourne (HCC, 2013a).

3.1.2 Polluted site: Kings Crescent, Lower Hutt

Tree sample KNG52 (52 Kings Crescent, Lower Hutt; Figure 3.10) was the location of a 14-metre high Kauri tree cut down in December 2012 by the Hutt City Council. Due to its urban locality and age (107 years old) of the tree, the potential for developing a local fossil fuel CO_2 record was realised and a slab of the tree was obtained.

Kings Crescent is located in central Lower Hutt in a densely populated urban area. Closely situated to the Westfield shopping mall, Hutt Hospital and State Highway 2, Kings Crescent sees high traffic flow. This site is expected to provide a 'polluted air' record due to its proximity to the urban environment. This record will be directly compared to the background record to investigate relative differences in $\Delta^{14}CO_2$ and to calculated CO_{2ff} emissions (Chapter 4.1.2 & 4.4.3).

Figure 3.10: KNG52, 52 Kings Crescent, Lower Hutt (HCC, 2013a)

3.2 Sampling strategy and core preparation

3.2.1 Core sampling

As the NIK trees are living trees it was necessary to extract a core that reached the centre of the trees with minimal damage. This was completed by Jocelyn Turnbull and Bjorn Johns. The cores, 5mm in diameter, were extracted using a Haglöf increment borer.

To obtain cores that contain all existing tree rings, the borer was pressed to the bark of the trees and screwed into the trunk by the operator. Once it reached the desired depth, the cores were removed by rotating the borer one half turn and withdrawing the cores using a long metal spatula inserted inside the instrument. As the core angle is difficult to gauge, the centres of the trees were not sampled.

The tree located at KNG52 was being felled so an entire cross section, or "cookie", of the tree was obtained. Acquiring a cookie from the tree was preferred as all rings were therefore available for sampling.

3.2.2 Dendrochronological analysis

Tree ring counting enables tree samples to be dated and aid the development of a dendrochronology. Annual tree rings represent a single year of growth that also reflects the climatic conditions in which they grew. Tree ring analysis for this study was completed by Dr Gretel Boswijk (University of Auckland).

The tree cores (NIK) and cookie (KNG52) were allowed to air dry before being sanded and scraped down with a scalpel in preparation for ring counting. This ensured that the surface was smooth and ring structures were visible. Typically during tree ring counting procedures, glue or some other adhesive is used, however, this step was purposely excluded as there is a risk of contaminating the wood for radiocarbon measurement. Ring boundaries were inspected under microscope and hand lens. Ring widths were measured on a set up comprised of a low-powered binocular microscope and a travelling stage connected via a linear encoder to a computer. Data captured by an input and cross-matching program (*Corina*; Cornell Tree-Ring Laboratory, 2012) were used to compare series statistically and visually. Each growth ring was counted, from the bark (current year) back to the centre, and assigned to the corresponding calendar year (Boswijk et al., 2014). It is vital that the outer most ring was identified accurately to ensure that each ring was assigned the appropriate year, otherwise the entire chronology would be incorrect.

3.2.3 Sampling method

After the tree rings were counted and the dendrochronology was established, individual rings were sampled in preparation for analysis. Using a scalpel, individual rings were sampled; special care was taken to sample only from the centre of the ring in order to avoid sampling from the years immediately before and after the target year. This proved to be difficult as the ring widths varied greatly (from ~1 mm to 10 mm), particularly in the KNG52 sample. The pieces of wood were then weighed and loaded into sample vials labelled with the sample identifiers. This task was completed by summer student Andrea Davies.

115 wood samples (62 x KNG52, 8 x NIK19 and 45 x NIK23) were analysed. The sampling intervals varied, chosen strategically to cover areas of interest (e.g. the "bomb spike" was targeted as confirmation of the established dendrochronology) and with emphasis placed on the more recent period of the record (1980s – present).

3.2.4 Standards

Subsamples of laboratory wood standards were created as required. These included a Kauri "blank" wood standard, which is >140,000 years old and thus contains no ^{14}C activity (Marra et al., 2006; Hogg et al., 2006; Norris, 2015). Several oak International Radiocarbon Inter-Comparison samples (SIRI-F and FIRI-D) were also used, the ages of which are approximately 530 and 4,500 years BP respectively but range across multiple years. However as it is pre-bomb there is an insignificant difference in ^{14}C content across all rings (Scott et al., 2003). These were treated the same as the "unknown" tree samples through to AMS analysis and were used as a representation of sample processing conditions. This helps determine how repeatable measurements of unknown samples are and aid in calculating uncertainties.

3.3 Physical and chemical pre-treatment of samples

Cellulose, particularly α-cellulose, is the favoured fraction of wood used in laboratory analysis techniques such as radiocarbon dating. Cellulose is the target material in the wood for analysis as it is directly related to formation of glucose by a tree during photosynthesis, and is considered the most reliable fraction in wood (Park & Epstein, 1961). After formation of cellulose, no further exchange of carbon with the atmosphere occurs. The cellulose component thus reflects the ^{14}C assimilated by the plant during photosynthesis, unlike the formation of lignin and starch, which takes place after cellulose has been formed (Fritts, 1976). To remove cellulose from a wood sample requires mechanical and chemical processing to remove lignin, extractives and non-cellulosic polysaccharides, leaving a pure cellulose component with the appropriate ^{14}C signature (Boettger et al., 2007). The method of sample preparation and cellulose extraction used in this study was developed by Norris (2015).

3.3.1 Physical pre-treatment

Each tree ring sample was inspected for fibres or other form of contamination, under a microscope. If present, contaminants were removed using a scalpel blade. Larger samples were subsampled, by cutting the sample longitudinally into the desired size for analysis. The subsampled piece was cut into silvers about 4-5mm long and 1mm wide. This was weighed, wrapped in Glass Fibre filter paper and placed in a glass thimble ready for chemical treatment. Any remaining sample was weighed and retained in the sample tube in case it was needed for repeat analysis.

3.3.2 Organic Solvent Washes (OSW)

The samples were chemically pre-treated with three chemical washes with a soxhelet extractor to remove resins, lipids and waxes from the wood. The Rafter OSW technique was employed, which involves three consecutive treatments using n-hexane, 2-propanol, and acetone (Norris, 2015). Each treatment takes ~120 minutes, at completion of all treatments the samples are rinsed with deionised (DI) water and dried in the 50ºC oven for at least two days. The dried samples were weighed and placed into centrifuge tubes, ready for cellulose extraction.

3.3.3 Cellulose Extraction

Norris (2015) demonstrated that for post-bomb wood, the ANSTO method of cellulose extraction was more effective than the standard Rafter Method at isolating the cellulose fraction. Therefore the ANSTO method was used on all wood samples. This method includes four steps usually performed on 12 samples over a two-day period.

Firstly, the solvent treated wood slivers were further treated to extract the holocellulose by bleaching the samples with $NaClO_2$ (15g/L) and 3ml 0.5M HCl (to adjust the solution to pH 2-3). The tubes were placed in a water bath heated to 90°C for 90 minutes, until the samples are white and no longer buoyant. The tubes were then centrifuged, decanted and filled with DI water, repeated until neutral.

The next two steps used NaOH washes to extract α-cellulose from the hollocellulose. First the samples were washed with 12%w/v NaOH under a nitrogen atmosphere at 60°C for 60 minutes, and then with 7%w/v NaOH solution under the same conditions. The samples were then rinsed to neutral pH.

The final step involved acidification of the samples with 2.0 M HCl at room temperature for 120 minutes, after which they were rinsed to neutral, decanted and dried in the 50°C oven. Once dried, the samples were weighed and then placed in glass tubes ready for combustion.

3.4 Conversion to CO_2 then graphite and AMS measurement

To measure the ^{14}C content of the cellulose, first the samples are combusted to CO_2. The CO_2 gas is then converted into carbon in the form of graphite that is ultimately measured via Accelerator Mass Spectrometry (AMS). These processes were completed at the Rafter Radiocarbon laboratory as part of standard laboratory procedure by various staff.

3.4.1 Elemental Analyser combustion and CO_2 collection

This process involved combustion of the pre-treated cellulose samples using a Europa ANCA elemental analyser (EA) connected to a Europa 20-20 mass spectrometer and a custom-built CO_2 collection device to produce CO_2 gas. The samples were weighed into tin capsules. The gas produced was then cryogenically purified and trapped into pneumatically operated sample bottles ready for subsequent graphitisation using an in-house developed collection device (Baisden et al., 2013a).

3.4.2 Graphitisation

The samples were graphitised at the Rafter Radiocarbon Laboratory using the hydrogen method as described in Turnbull et al., (2015). The prepared CO_2 gas samples were transferred to the Rafter Graphitisation 20 reactor system (RG20). Initially, ~2.8mg of iron catalyst was prepared by reducing Fe_2O_3 to pure iron (Fe) by reaction with ~1300 mbar of H_2 gas at 400°C. Following this reaction, the sample CO_2 aliquot was introduced into the reactor. The CO_2 pressure was measured, allowing the calculation of the number of moles of gas produced. 2.3 moles of hydrogen gas for every 1 mole of CO_2 was added to the reactor (a slight excess relative to the 2:1 ratio needed for complete reaction). The CO_2 gas was converted into carbon in the form of graphite over the reduced iron (Fe) catalyst at 550°C. Water vapour produced during the reaction was frozen out as an ice pellet using a thermoelectric cooler to drive the reaction to completion. The reaction (Equation 3.1) proceeded for approximately 2-3 hours until pressure stabilised, signifying completion. Final pressure was checked (within tolerances) that it was as expected from the initial CO_2 and H_2 pressures and reaction was complete (Turnbull et al., 2015). The graphitisation reaction is described with the following equation:

$$CO_2 + 2H_2 \underset{Fe}{\rightarrow} 2H_2O + C_{graphite} \qquad (3.1)$$

The graphitised samples were placed into cleaned plastic vials until AMS measurement.

3.4.3 AMS Measurement

When ready for analysis, the graphitised samples were packed into aluminium targets (cathode holders) prior to AMS measurement. The graphite samples were analysed via mass spectrometry using the 0.5 MV NEC Extended Compact Accelerator Mass Spectrometer (XCAMS) housed at NIC (Baisden et al., 2013a; Zondervan et al., 2015). Each ^{14}C measurement wheel contained 40 graphite targets including two tuning targets (one modern and one Kapuni CO_2 blank), eight Oxalic Acid I primary standards, two BHD ambient air samples and two wood blanks (Kauri and SIRI), the remainder made up of unknown samples.

The ^{14}C content of each sample was determined using the in-house CALAMS processing software. The resultant data was normalised $\delta^{13}C$ of –25‰ (Zondervan et al., 2015). A process blank correction was applied using the processing blank Kauri wood measured during the same time period (Donahue et al., 1990; Turnbull et al., 2015). Results were reported as fraction modern, $F^{14}C$ (determined by the ratio of activity of the sample versus that of the standard that has been background corrected and normalised to $\delta^{13}C$ of –25‰ (Reimer et. al., 2004) and as $\Delta^{14}C$ (based on the $F^{14}C$ and decay corrected to the date of collection; Stuiver & Polach, 1977).

CHAPTER 4: RESULTS AND DISCUSSION

4.1 Tree Ring Results

4.1.1 Background sites; Baring Head $^{14}CO_2$ record and NIK tree $^{14}CO_2$

The Baring Head atmospheric $^{14}CO_2$ record provides a reliable dataset to validate the $^{14}CO_2$ tree ring record developed as part of this study (Currie et al., 2011; Turnbull et al., 2014a). A smooth curve fit was applied to the BHD $^{14}CO_2$ dataset and a time-varying one-sigma uncertainty on this smooth curve was determined using a Monte Carlo analysis of the individual measurements and their uncertainties (Turnbull et al., 2014a).

It is important to determine whether the tree rings sample the atmosphere in a reproducible manner. Once this is established, the technique can be applied to the samples collected from the polluted test site (KNG52). An annual record of ^{14}C was measured from the tree rings sampled from the two cores NIK19 and NIK23. To demonstrate the agreement of tree ring results to atmospheric $^{14}CO_2$ atmospheric, the tree ring $^{14}CO_2$ measurements were compared to the BHD dataset (Figure 4.11).

Replicating the bomb spike in the tree ring records is important to ensure that the ring counts are correct and that the trees are reliably sampling the atmosphere. Immediately preceding the bomb spike, the NIK $^{14}CO_2$ record replicates the BHD $^{14}CO_2$ record well, ensuring that the ring count chronology is correct (Figure 4.11). During the bomb spike however (here referring to the 1965 – 1967 period), the $\Delta^{14}CO_2$ values in the NIK record are notably lower than $\Delta^{14}CO_2$ values from BHD. Throughout this period atmospheric ^{14}C was changing at an extremely rapid rate, as seen in the BHD record, which is constructed from samples collected over typically two week periods at roughly monthly intervals. As the NIK samples are an average annual measurement, representative of the summer period only, it is possible the tree ring samples are not representing interannual variability that shorter term samples (such as those used to construct the BHD record) would.

There are three possible explanations for the seemingly lower measurements during the 1995 – 2005 period: the tree rings do not accurately reflect atmospheric ^{14}C, a possible ring counting error, or a bias in the BHD atmospheric $^{14}CO_2$ record (Figure 4.12). As the NIK data accurately reproduces the period immediately preceding the bomb spike, it is clear the tree is accurately sampling the atmosphere and the ring count chronology is correct.

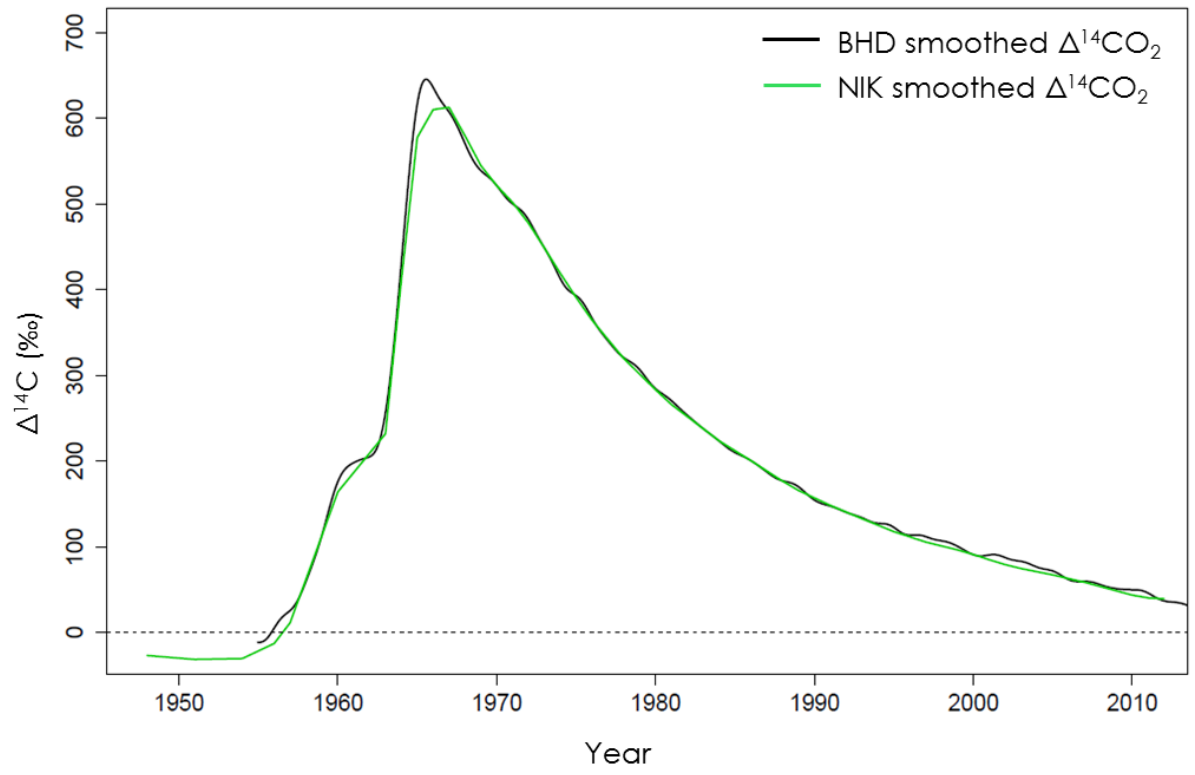

Figure 4.11: Smooth curve from NIK data compared with BHD clean air record. The tree ring data agrees well with the BHD $\Delta^{14}CO_2$ data, establishing that the trees are sampling $^{14}CO_2$ accurately from the atmosphere. There are two notable periods where the tree ring data is slightly lower than the $^{14}CO_2$ record, during the bomb spike and in the period between 1995 & 2005 (Figure 4.12).

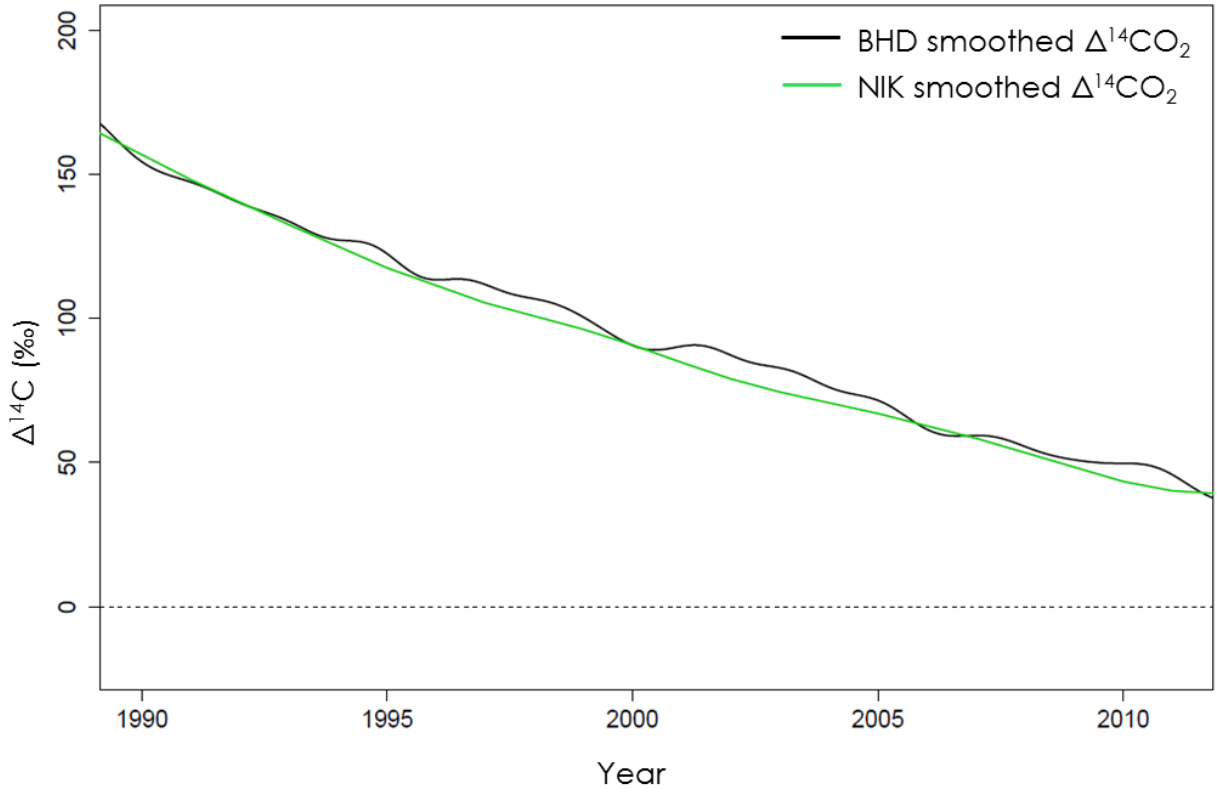

Figure 4.12: NIK data compared with BHD clean air record (Turnbull et al., 2014a) for the period 1990 to 2012. The disagreement in values is a suspected bias in the BHD record.

The offset during the 1995 – 2005 period has been observed in previous studies (Currie et al., 2011; Turnbull et al., 2014a) and it is believed that the $\Delta^{14}CO_2$ measurements for the 1995 – 2005 are higher than expected caused by either a bias in the sample collection or in the AMS measurements (Turnbull et al., 2014a). An earlier version of the $^{14}CO_2$ data set (Currie et al. 2009) had a period of anomalously high ^{14}C values between 1990 – 1993, which has been revised lower by Turnbull et al. (2004a) using evidence from new measurements of archived flask samples. The tree rings analysed here confirm the lower values for the 1990 – 1993 period (Norris, 2015). In the early part of the BHD $^{14}CO_2$ record ^{14}C was quantified by gas proportional counting, which measures disintegration of β particles. However after May 1995, measurements were made by counting of the number of $^{14}C/^{12}C$ atoms using AMS. Early measurements were made in the infancy of radiocarbon and the measurements were subject to large variations due to measurement uncertainties, high variability of ^{14}C around the peak of the bomb curve and sparse measurements in some years. The trees analysed here confirm that the time period 1995 – 2005 new XCAMS measurements tend to be lower than the data used in the previously published version of the atmospheric record (Currie et al. 2009) and this data may also be revised lower as a result (Turnbull et al., 2014a; Norris, 2015).

4.1.2 Polluted site; KNG52

As the NIK tree samples showed excellent replication of the BHD atmospheric record, the tree ring method was established as an accurate tool to reproduce historic $\Delta^{14}CO_2$ values, the method was then applied to the tree at the test site in central Lower Hutt. Due to its urban location, it was presumed that this tree would receive CO_{2ff} emissions from the surrounding area, thus providing a "polluted" record of $^{14}CO_2$.

Initial measurements showed poor agreement during the pre-bomb and bomb spike periods (Figure 4.13). This was initially thought to be a localised effect caused by the terrestrial biosphere. However, shifting the record along the time axis identified a suspected ring counting error. The tree sample was re-investigated and a missing tree ring was identified, suggesting that the sample originally determined as 1989 was in fact a combination of rings 1989 and 1988 and that no independent sample of 1988 was made. Thus, all older samples were biased by one year. This was confirmed by Dr Gretel Boswijk (UoA) and the record was amended to include the new chronology, where the 1989 sample was omitted and all preceding samples were relabelled.

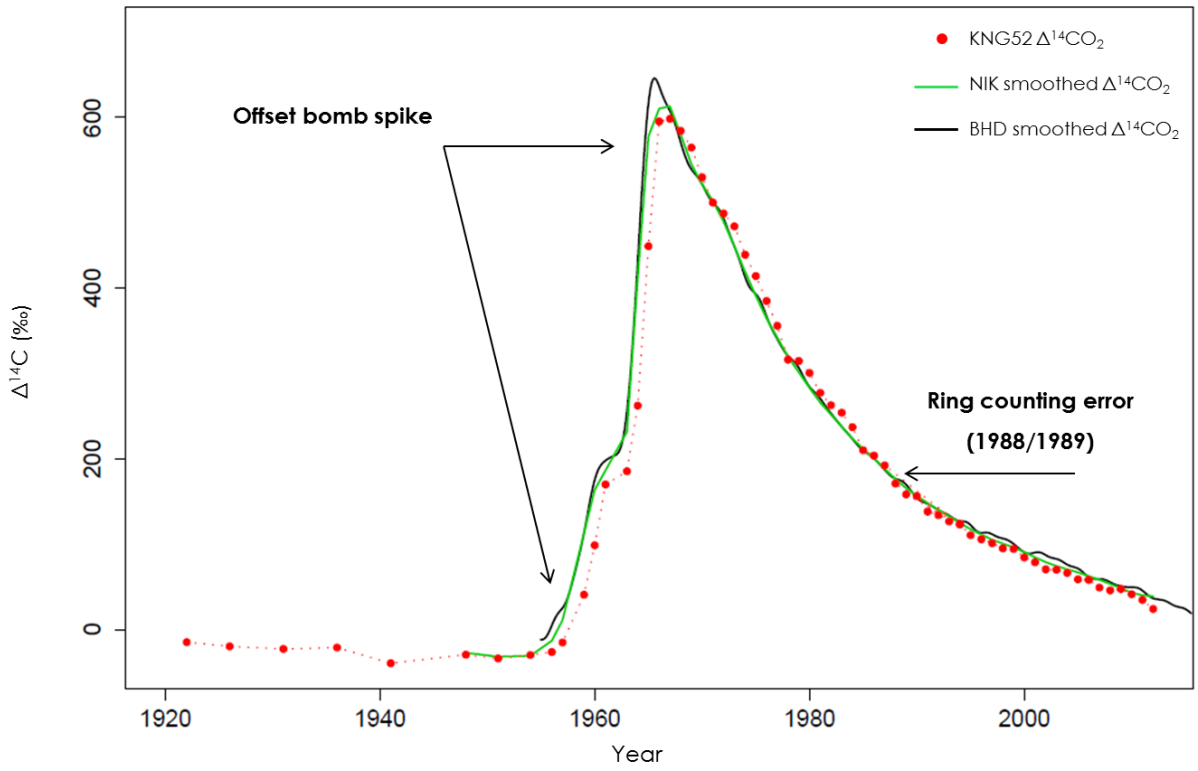

Figure 4.13: The initial comparison between the KNG52 $\Delta^{14}CO_2$ measurements and the NIK and BHD $^{14}CO_2$ records showed poor agreement between the 1960 and 1980 period.

4.2 Timeline of radiocarbon distribution

Once the correct chronology was established, the ^{14}C data from the KNG52 samples were compared comprehensively to the NIK and BHD $^{14}CO_2$ records (Figure 4.14). The radiocarbon timeline was defined by four distinctive time periods; pre-bomb, bomb period, post-bomb and fossil-era, which is elaborated on in the following sections.

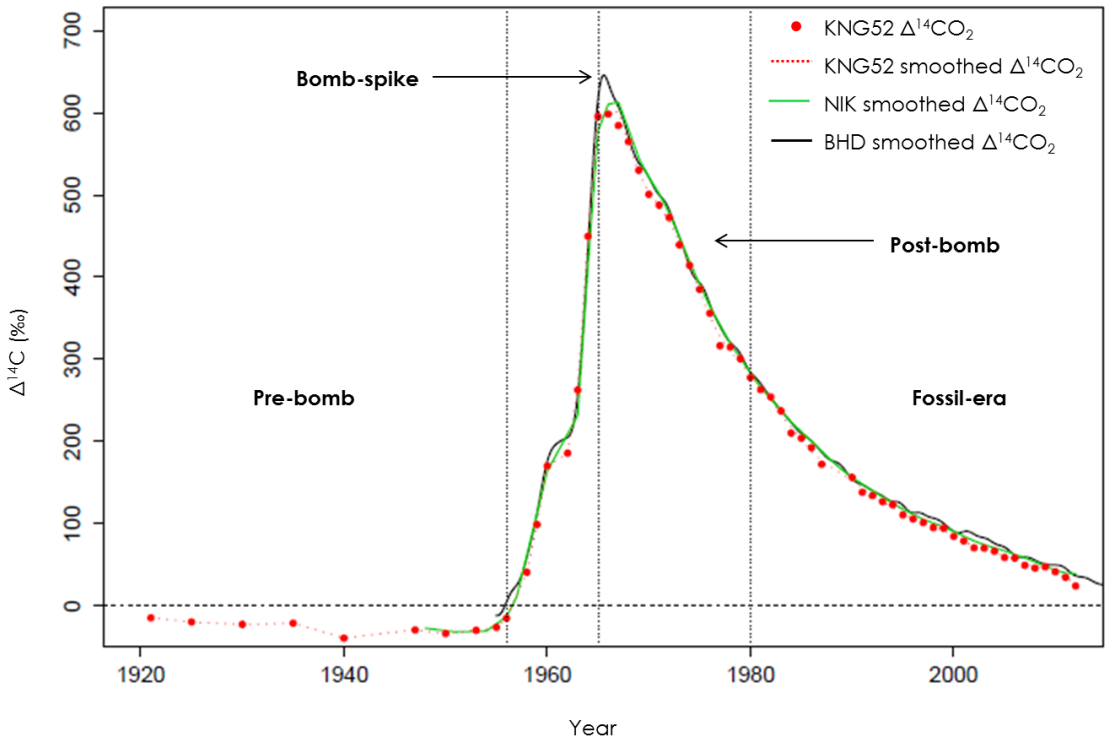

Figure 4.14: KNG52 Δ14CO2 measurements compared with the NIK and BHD 14CO2 atmospheric curves, here defined by four time periods; pre-bomb, bomb period, post-bomb and fossil-era.

4.2.1 Pre-bomb

Pre-1956, a natural level of ^{14}C existed with cosmogenic production approximately balancing radioactive decay with very little influence from the biosphere and CO_{2ff} emissions (Figure 4.15A). It was expected that the KNG52 measurements would follow the NIK and BHD records very closely. In the period immediately prior to the instigation of nuclear bomb testing in the mid-1950s, the KNG52 values were persistently recording a $\Delta^{14}CO_2$ of ~-25‰. This is consistent with other pre-bomb tree ring records (Hua & Barbetti, 2004; Rakowski, 2011; Hua et al., 2013) and is likely to be caused by a combination of a small amount of post-industrial revolution fossil fuel combustion (the *Suess Effect,* as described in Chapter 2.3.2; Suess, 1955; Schuur et al., 2016).

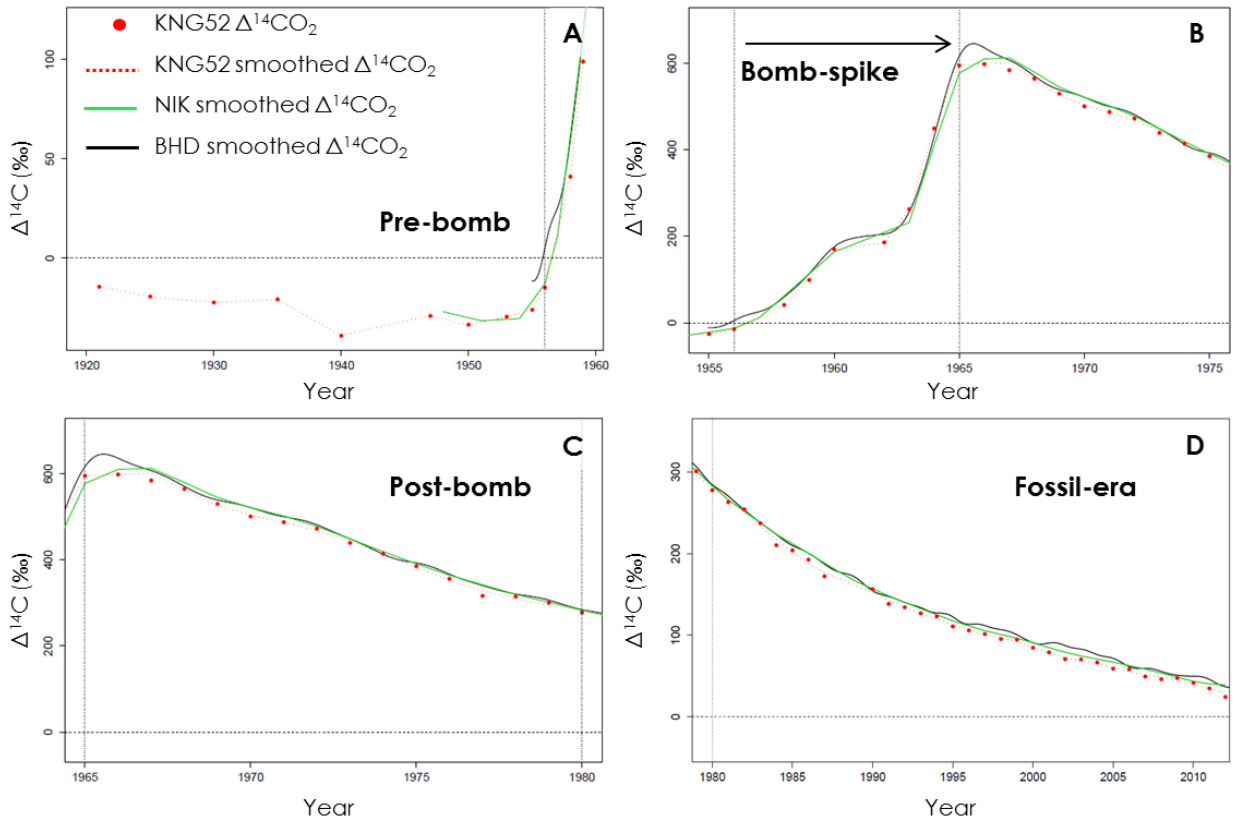

Figure 4.15: **A** – Pre-bomb, characterised by cosmogenic production approximately balancing radioactive decay; **B** – The bomb period, a rapid increase in atmospheric $\Delta^{14}C$ due to an injection of nuclear bomb ^{14}C into the atmosphere; **C** – Post-bomb, a period of rapid uptake of $^{14}CO_2$ by the oceans and biosphere (Hua et al., 2013); **D** – Fossil-era, the KNG52 record exhibited lower $\Delta^{14}CO_2$ values than the BHD record, consistent with an increase in local CO_{2ff}.

4.2.2 The bomb period

During the bomb period, here defined as the period 1956 to 1965, there was a rapid increase in atmospheric $\Delta^{14}C$ due to the influence of aboveground nuclear detonations. The KNG52 measurements show generally good agreement with the BHD and NIK $\Delta^{14}CO_2$ data of the corresponding year (Figure 4.15B). An exception of this is the data point associated with the year 1961, which is noticeably lower than that seen in the background records. Additionally, as previously observed in the NIK record, the bomb spike period is characterised by lower values of $\Delta^{14}CO_2$ in the KNG52 record compared with those presented in the BHD record. As discussed earlier in reference to the NIK record not accurately replicating the bomb spike seen in the BHD record, this is likely to be due to the rapid changes in $^{14}CO_2$ not being accurately sampled by the summer-averaged annual data received from a single tree ring.

4.2.3 Post-bomb

The post bomb period, from 1965 to 1980, is generally characterised as a period of rapid uptake of $^{14}CO_2$ by the oceans and biosphere based on previous studies (Hua et al., 2013). During this period the KNG52 data varies from closely following the BHD record to slightly lower values (Figure 4.15C). The tendency for lower $\Delta^{14}CO_2$ values could be anomalous measurements due to inconsistent sampling from the tree rings (as described in Chapter 4.2.1). Alternatively, the lower values in the KNG52 $^{14}CO_2$ record during this period could be an indication of an early onset expression of increased fossil fuel CO_2, however, changes in emissions were not likely to be very significant during the 1960s and 1970s. Over the long record, the influence of the terrestrial biosphere changes dramatically due to the rapid increase in bomb injected ^{14}C in the atmosphere, therefore, it is possible that the variability in the $\Delta^{14}CO_2$ measurements during this period is an indication of the influence of the terrestrial biosphere.

Calculations of the CO_{2ff} and CO_{2r} contributions to discern the source of ^{14}C should confirm the relative influence of the biosphere. A model simulation of added biosphere correction to BHD was calculated to predict KNG52 $\Delta^{14}CO_2$ (Δ_{obs}) in the absence of fossil fuels, where biosphere was the only contribution (Δ_{obs1}; $CO_{2ff} = 0$).

We revisit equation 2.7:

$$CO_{2ff} = \frac{CO_{2obs}(\Delta_{obs} - \Delta_{bg})}{\Delta_{ff} - \Delta_{bg}} - \frac{CO_{2other}(\Delta_{other} - \Delta_{bg})}{\Delta_{ff} - \Delta_{bg}}$$

(2.7)

And then solved for Δ_{obs1}:

$$\Delta_{obs1} = \frac{(CO_{2bg} \times \Delta_{bg}) + (CO_{2ff} \times \Delta_{ff}) + (CO_{2r} \times \Delta_{r}) + (CO_{2p} \times \Delta_{p})}{CO_{2obs}}$$

(4.1)

Where:

Δ_{obs1} = observed $\Delta^{14}CO_2$ value at KNG52 if biosphere was the only influence

$CO_{2ff} = 0$

CO_{2r} = 4.25 ppm, net respiration flux (Baisden et al., 2013b)

$\Delta_r = \Delta^{14}C$ value of biospheric flux, assumed to be background flux value of 17 years prior

CO_{2p} = -4.25 ppm, assuming a neutral biosphere, where p balances r

$\Delta_p = \Delta_{bg}$

$CO_{2obs} = CO_{2bg} + CO_{2ff} + CO_{2r} + CO_{2p}$

We chose CO_{2r} based on research conducted by Baisden et al., (2013b), which calculated a net respiration flux for the Hutt Valley of 4.25 ppm of CO_2 per day (converted to the mole fraction value using the method described in Turnbull et al., 2006b; 2009). The Δ_r value is assumed to be the atmospheric $\Delta^{14}C$ value of 17 years prior, based on estimates of a soil carbon residence time of 17.2 years (Judgeford, Hutt Valley; Baisden et al., 2013c; 2013d). This value dictates how old the carbon is that is being respired by the biosphere at any time. It is assumed that this is at steady rate.

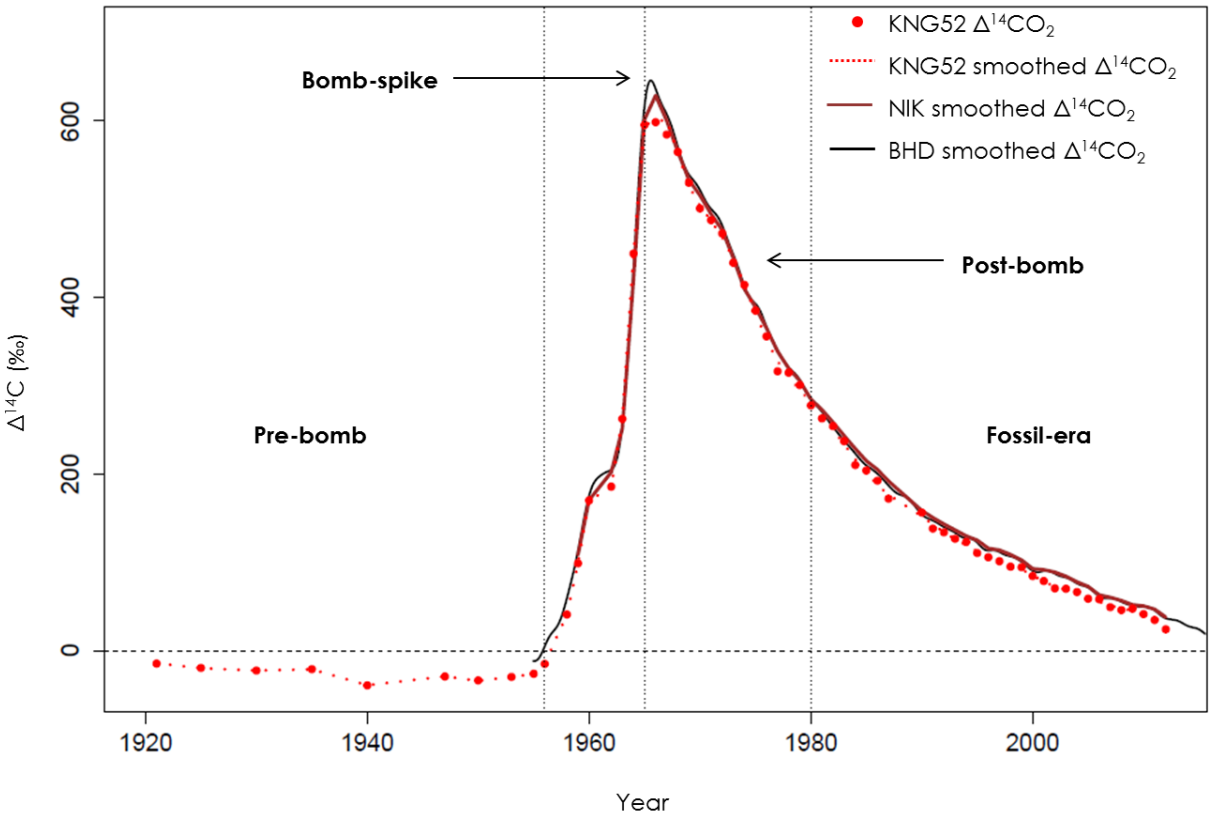

Figure 4.16: Calculated KNG52 $\Delta^{14}CO_2$ in the absence of fossil fuel emissions (A.1).

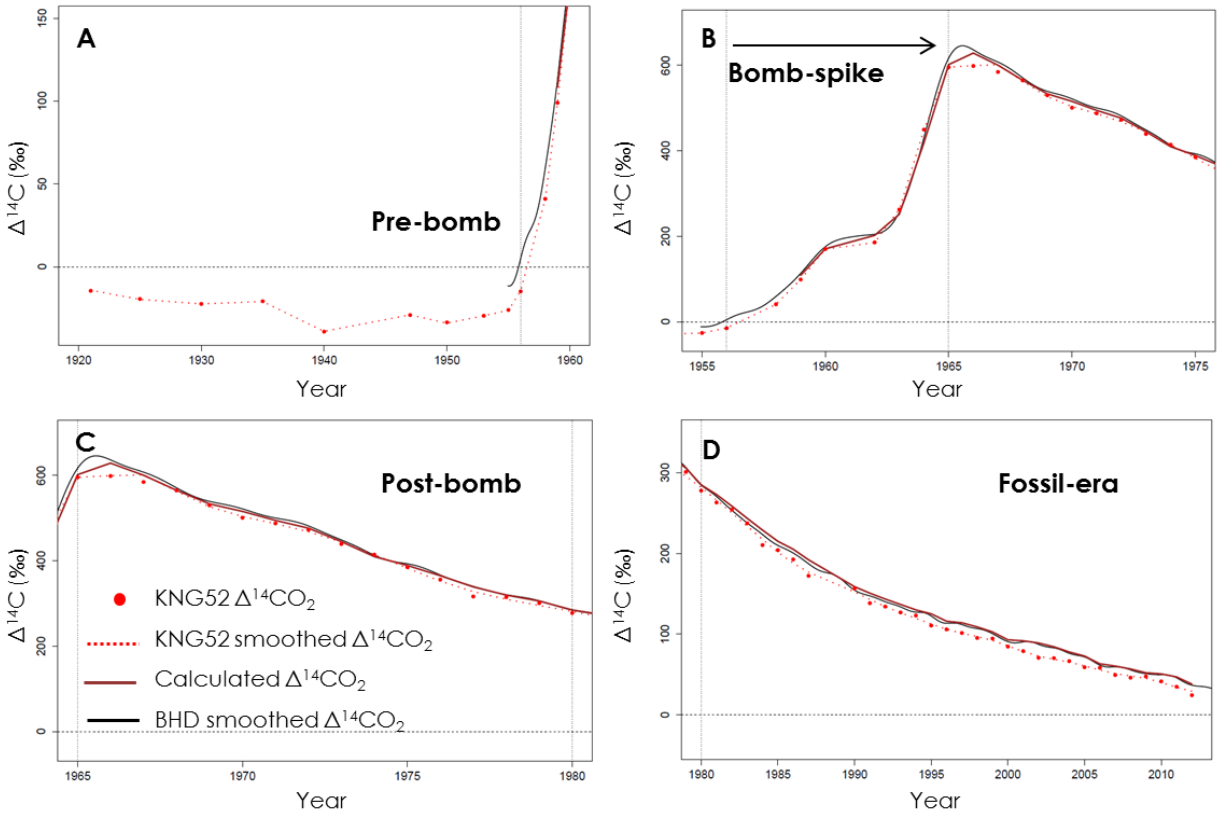

Figure 4.17 - **A** – Pre-bomb, calculated $\Delta^{14}CO_2$ follows the BHD and KNG52 records; **B** – The bomb period, preceding the bomb spike, the calculated $^{14}CO_2$ record followed the BHD and KNG52 records closely; **C** – Post-bomb, the calculated $\Delta^{14}CO_2$ showed slightly lower values then the BHD record; **D** – Fossil-era, the calculated $\Delta^{14}CO_2$ record exhibits slightly higher values then KNG52 and BHD.

The calculated KNG52 $\Delta^{14}CO_2$ showed that in the absence of fossil fuels, and when biosphere was in theory the only influence on $\Delta^{14}CO_2$, the measurements would closely follow the BHD $^{14}CO_2$ record (A.1). With the exception of a brief period from 1960 to 1962 and the bomb spike, the biosphere had very little effect. During the post-bomb period variability in the KNG52 record is likely to be caused by the effect of the local biosphere. From the 1980s onward, calculated $\Delta^{14}CO_2$ shows slightly higher values then the KNG52 and BHD record. The fact that the KNG52 record deviates quite significantly at this point show that CO_{2ff} becomes the dominant driver of the $\Delta^{14}CO_2$ from the 1980s onward. Thus, it is acceptable to say that the dominate driver of the KNG52 $^{14}CO_2$ record, particularly from the 1980s onward, is fossil fuel emissions.

4.2.4 Fossil-era

From 1980 to 2012 the KNG52 record presents persistently lower values than the BHD record, with some variability throughout (Figure 4.15D & 4.18A). A decrease in $^{14}CO_2$ is consistent with an increase in CO_{2ff} in the atmosphere, with additions of fossil fuel CO_2 become the dominant driver of the $^{14}CO_2$ from the 1980s onward. The comparison with the biosphere only model shows that CO_{2ff} is the cause of the lower values since 1980 (Figure 4.18B).

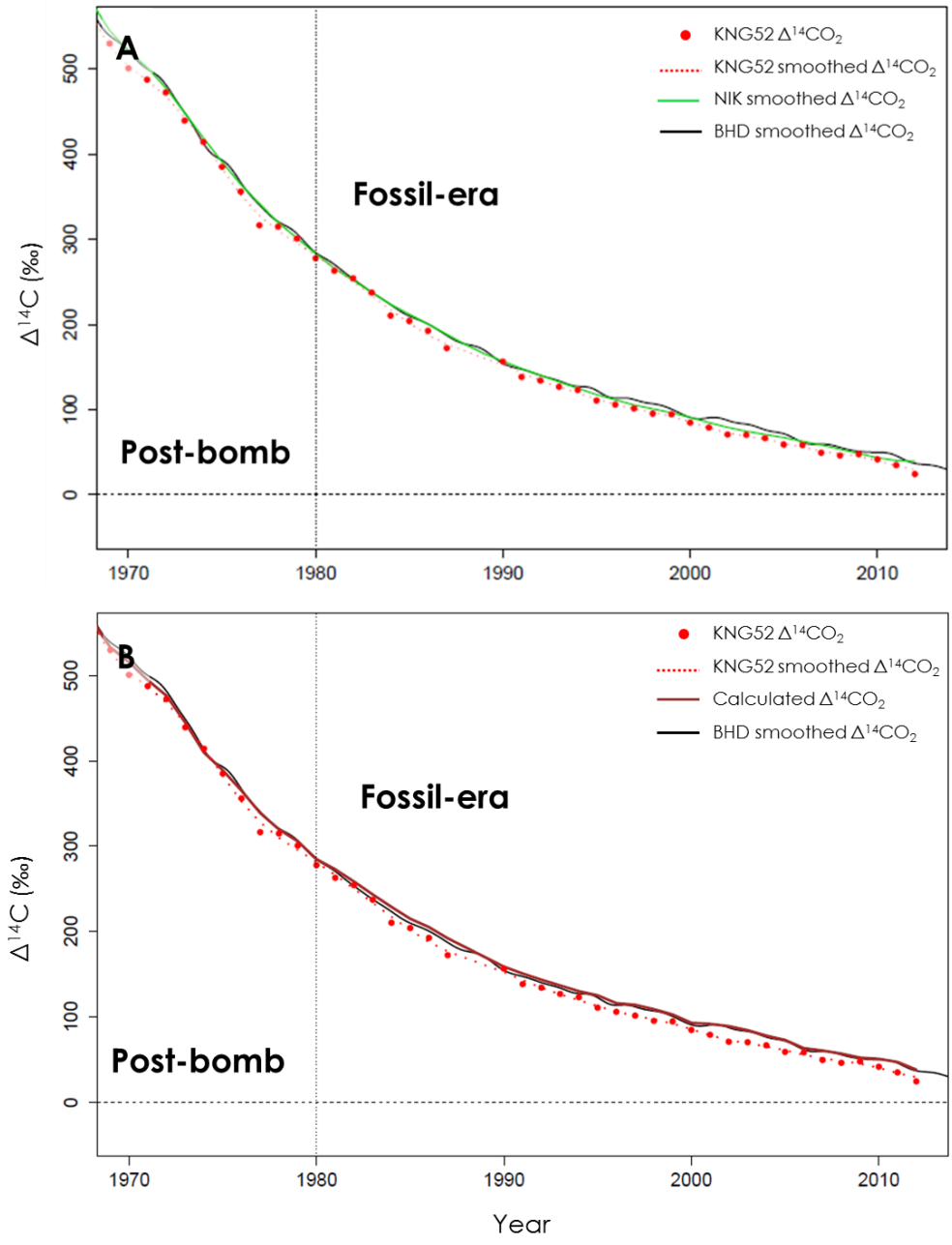

Figure 4.18: **A** - KNG52 $\Delta^{14}CO_2$ measurements compared with the NIK and BHD $^{14}CO_2$ atmospheric curves for period 1970 to 2012. From 1970 to 1980 the KNG52 record presents periods of lower values relative to the background records. From 1980 to 2012, the KNG52 measurements are consistently lower than the background measurements. **B** - Calculated observed $^{14}CO_2$ consistently follows the BHD $^{14}CO_2$ record during this period demonstrating that CO_{2ff} is the cause of the lower values since 1980.

4.3 Calculation of CO_{2ff} from ^{14}C data

4.3.1 Calculating CO_{2ff}

Calculations were only possible back to 1972 due to limitations of available Δ_r data (BHD $^{14}CO_2$ record only goes back to 1955, which is 17 years prior to 1972). It would have been possible to assume a constant value of Δ_r prior to 1955, however, calculations showed that the biosphere correction was larger than CO_{2ff} in the earlier period, thus prior to this the calculations become redundant.

CO_{2ff} was calculated using the KNG52 $\Delta^{14}CO_2$ measurements utilising equation 2.8 (A.2):

$$CO_{2ff} = \frac{CO_{2bg}(\Delta_{obs} - \Delta_{bg})}{\Delta_{ff} - \Delta_{bg}} - \frac{CO_{2r}(\Delta_r - \Delta_{obs})}{\Delta_{ff} - \Delta_{obs}}$$

(2.8)

To apply the BHD CO_2 and $^{14}CO_2$ concentration data to calculate CO_{2ff} of the tree ring data, the data was averaged over an 8 month period from September to April. This was completed in order to replicate CO_2 concentrations during the growing season, when the cellulose was laid down.

4.3.2 Calculating the biosphere correction

In order to calculate the CO_{2ff} of observation years, it is necessary to calculate the relative effect of the biosphere on the $^{14}CO_2$ signal. The second term of the equation above is essentially a correction factor for all other sources of CO_2 (β). As already established for this particular study, the effect of nuclear power plants, ocean flux, photosynthesis or cosmogenic production of ^{14}C do not need be included in the calculation (Chapter 2.2.3). Therefore the only "other" effect on the CO_{2ff} signal is biospheric respiration, which needs to be accounted for using the following equation (A.3):

$$\beta = \frac{CO_{2r}(\Delta_r - \Delta_{obs})}{\Delta_{ff} - \Delta_{obs}}$$

(4.2)

Where:

CO_{2r} = Net respiration flux (Baisden et al., 2013b)

$\Delta_r = \Delta^{14}C$ value of flux, assumed to be background flux value of 17 years prior

Δ_{ff} = -1000‰

4.3.3 CO_{2ff} results

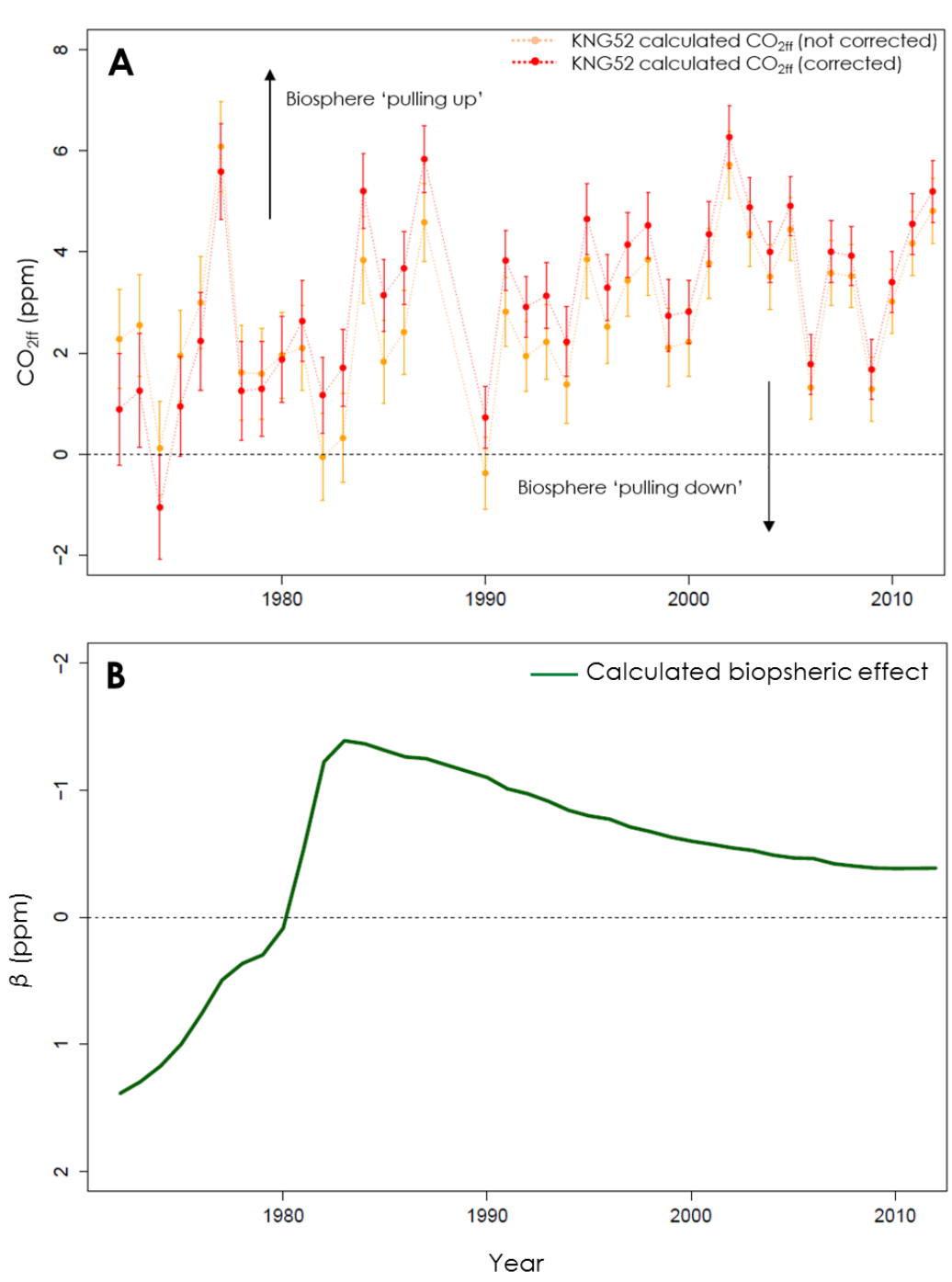

Figure 4.19: **A** - Calculated CO_{2ff} versus calculated CO_{2ff} that has been corrected for the biosphere influence (Chapter 4.4.2). Prior to 1980, the biospheric influence had the effect of 'pulling up' the CO_{2ff} record. From 1980 onward the biosphere has the effect of 'pulling down' the CO_{2ff} record. **B** - Calculated biosphere correction (Chapter 4.4.2) shows a positive influence until 1980 where it becomes negative.

The CO_{2ff} calculations were made for the KNG52 tree using the mass balance equation (Equation 2.8) for the period 1972 – 2012 and corrected for the biospheric effect using the respiration calculation (Equation 4.2; Figure 4.19). The calculated biosphere correction (calculated in Chapter 4.4.2) was plotted in comparison to calculated CO_{2ff} (Figure 4.19B). Prior to 1980, the biosphere was 'pulling up' the CO_{2ff} record. The biosphere at this time has a positive influence that has the effect of drawing down the CO_{2ff} signal, suggesting that it was the dominant driver of the KNG52 $^{14}CO_2$ record during this time. From 1980 this effect reversed phase and the biosphere was 'pulling down' the record (Figure 4.19A). The biosphere signal becomes negative, indicating that the fossil fuel CO_2 contribution becomes the dominant driver of CO_2 variability post-1980.

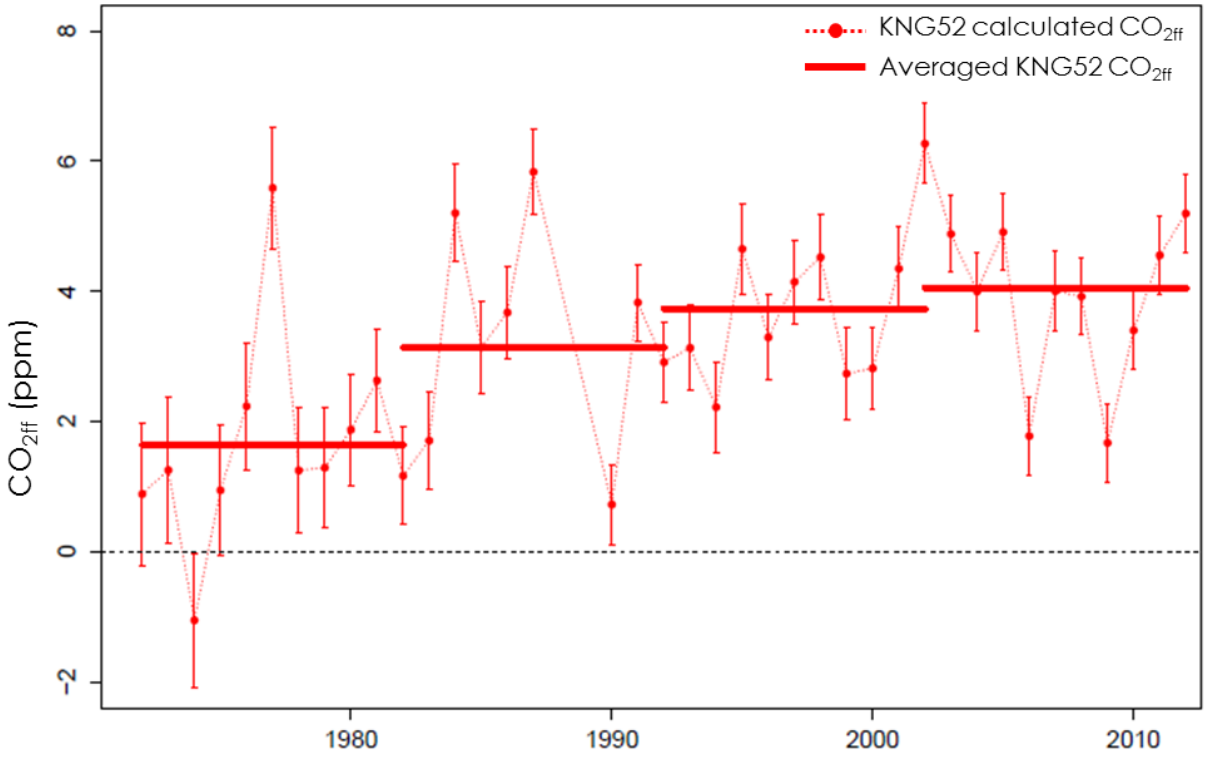

Figure 4.20: Calculated CO_{2ff} values from KNG52 $\Delta^{14}CO_2$ data. This shows a definite trend of increasing CO_{2ff} over time, approximately increasing by a factor of 2.4 over the 40 year period. Data averaged over 10 year periods is also plotted.

The calculated CO_{2ff} values increased from 0.9 ± 1.1 ppm in 1972 to 5.2 ±0.61 ppm in 2012 with some notable variability (fluctuating between -1.05 ±1 and 6.3 ±0.6 ppm) over the 40 year period. The calculated CO_{2ff} values were averaged over 10 year periods to clarify trends in the data (Figure 4.20; T4.1).

10 year average of calculated CO_{2ff}

Time period	*Average calculated CO_{2ff} (ppm)*
1972 – 1982	1.6 ±1.6
1982 – 1992	3.1 ±1.7
1992 – 2002	3.7 ±1.2
2002 – 2012	4.0 ± 1.4

(T4.1)

Over the long record, the CO_{2ff} increased by a factor of 2.5 (150%). The largest proportion of this increase occurred during the 1972 to 1992 period, increasing from 1.6 ±1.6 to 3.1 ±1.7, increasing by a factor of 1.9 (112%). From 1982 to 2002 the CO_{2ff} signal increased from 3.1 ±1.7 to 3.7 ±1.2, representing a 20% increase. Then from 1992 to 2012 there was only a 10% increase in CO_{2ff}, from 3.7 ±1.2 to 4.0 ± 1.4.

There is some periods of large variability throughout the record, particularly during the 1982 – 1992 period. In addition to the two missing data points (1988 and 1989), this period was poorly represented by very narrow rings and thus small samples. A sampling error where the full annual tree ring was not represented by the sample is likely. Some rings were particularly hard to sample due to the amount of wood available (ring widths varied significantly), thus it is possible that the $\Delta^{14}CO_2$ measurement could be biased toward the year immediately preceding (or succeeding) the year that it should correspond to. Therefore, sampling during this period is not particularly reliable and has resulted in large scatter. If this part of the record is ignored we can address two obvious trends in the data: low average values of CO_{2ff} (1.6 ±1.5) in the period 1972 – 1983 and higher values of CO_{2ff} (3.8 ±1.1) in the period 1991 to 2012. There is an overall increase of 140% over these two time periods.

4.4 Assessing variability in the record

4.4.1 Meteorological data

Meteorological data (wind speed and direction) were analysed to assess variability in the KNG52 CO_{2ff} record. Existing wind data from the Lower Hutt region only spanned the period 2005 – 2012 , however meteorological data collected from a site located at the Wellington Airport (16 km from test site; NIWA, 2016) spans the period 1970 to 2012.

Wind roses were constructed from data provided by both datasets for the period 2005 – 2012 (Figure 4.21). Hourly wind data was restricted to daylight hours (6:00 to 18:00 local time) between September and April to represent wind speed, direction and frequency during growing season. The dominant prevailing winds in Lower Hutt were determined as North Easterly (NE; 0° – 60°) and South Westerly (SW; 180° – 240°). At the Airport site they were Northerly (N; 330° – 30°) and Southerly (S; 150° – 210°). This difference in wind direction is likely due to the landscape formation of the Hutt Valley (Figure 4.22). The two separate wind types at each location occurred at similar proportions at each site; therefore it was reasonable to use the N-S wind directions from the Airport site as a wind direction proxy for the NE-SW wind directions Lower Hutt respectively.

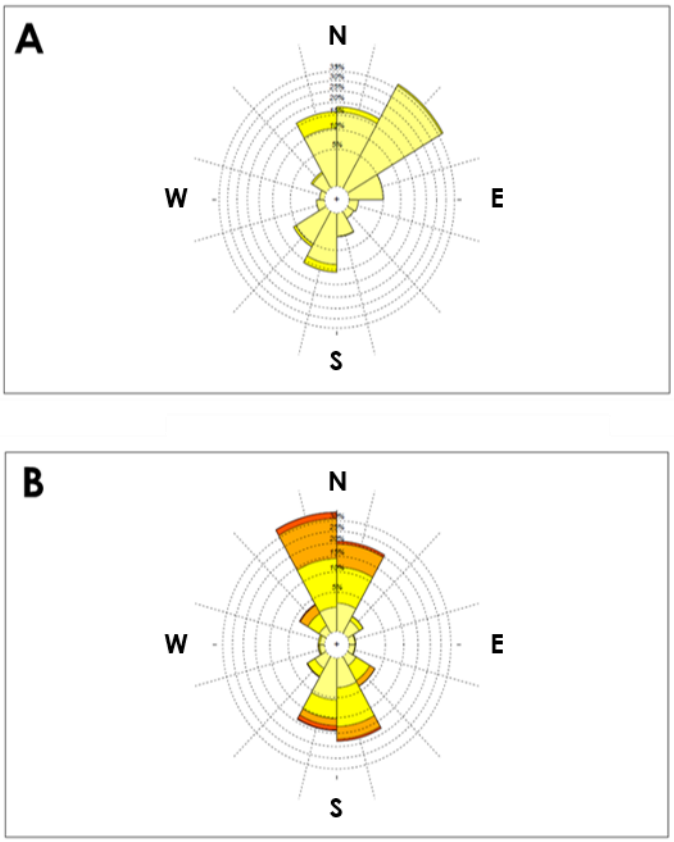

Figure 4.21: Wind roses representative of average wind speed (knots) from stations located at Lower Hutt (**A**; McGavin, 2016) and the Wellington Airport (**B**; NIWA, 2016) for the period 2005-2012.

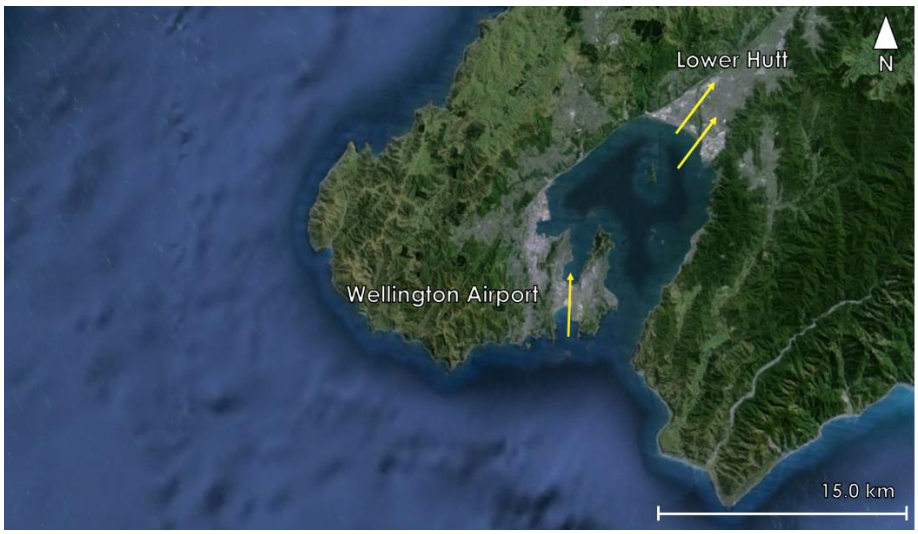

Figure 4.22: Wind direction in Lower Hutt versus Wellington Airport. Wind tunnels through the Wellington Harbour on a N-S trajectory, however it is forced into a NE-SW trajectory through the Hutt Valley due to the NE-SW position of the surrounding hills.

The hourly wind speed data from both sites for the 2005 – 2012 period were compared via a linear regression (Figure 4.23). The regression coefficient determined that the wind speeds measured at the airport were in general 60% higher than wind speeds measured at Lower Hutt (r^2=0.8). Multiplying the Airport data by the regression coefficient will provide a reasonable proxy for the Lower Hutt wind data not available. For the sake of continuity, airport data will be used for the period 1970 – 2012 with the two prevailing wind types (N and S) as a proxy for the Lower Hutt wind types (NE and SW) and the wind speeds from the Airport will be corrected based on the regression coefficient, to make comparisons with the CO_{2ff} data.

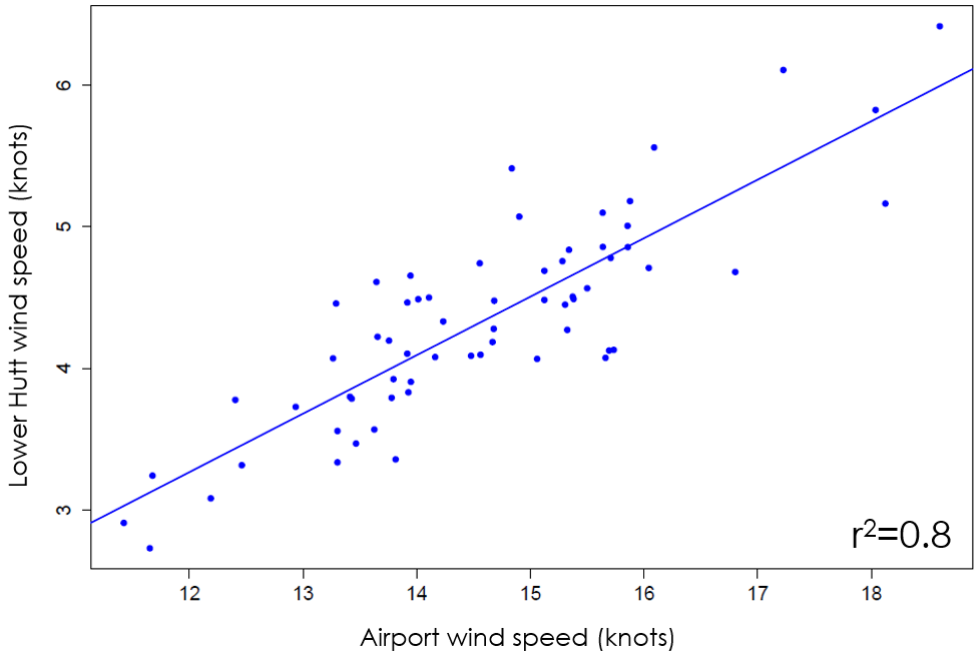

Figure 4.23: Regression plot of hourly wind speed data from the Lower Hutt and Airport sites.

To assess how wind patterns might affect atmospheric transport of CO_{2ff}, the wind data information was sorted into the relative frequency of the two wind types, average annual wind speed and the average annual wind speed of the two prevailing wind types (Figure 4.24). These were compared directly with the KNG52 CO_{2ff} record.

The dominant prevailing wind is Northerly, occurring ~50% of the time. Southerly winds occurred less but also often at ~30% of the time. The remaining ~20% of cases were made up of wind directions outside the chosen ranges and calm conditions (below 2 knots; Figure 4.24B). Analysis of the temporal change in meteorology showed that there was little interannual variability in wind direction and the comparison revealed no relationship to trends in the KNG52 CO_{2ff} record (Figure 4.24A).

A mean annual wind speed plot was constructed (Figure 4.24C), which determined a mean wind speed that fluctuated between 6 and 7 knots from 1970 to 1988 (with an average of 6.7 knots over the 18-year period). A comparison of average wind speeds for the two wind types was made (Figure 4.24C). Both the Northerly and Southerly wind speed records follow a very similar pattern to that expressed in the average wind speed data, therefore average wind speed was appropriate to be used in analysis. There was a peak in mean wind speeds from 1989 to 1993, with mean wind speeds increasing to an average of 7.3 knots. During the period of high wind speeds (1989 – 1993) there is a drop in CO_{2ff} observed, particularly at 1990. However, as the data points for the years 1988 and 1989 do not exist in the CO_{2ff} record, a comprehensive comparison cannot be made for this period.

From 1994 to 2012, the mean wind speed experienced a slight drop to an average 6.1 knots. This represents a 10% decline in average wind speed from the early part of the record (1972 – 1987). There is a marked increase in the CO_{2ff} record during this period (1994 – 2012), compared to the earlier part of the record (1972 – 1987; Figure 4.24A). The average CO_{2ff} values increase from 2.4 ±1.9 ppm to 3.9 ±1.2 ppm, increasing by 60%. If the mole fraction increase in CO_{2ff} was solely due to the drop in wind speeds (implying an inverse relationship), then it would be expected that the magnitude in change in both records would scale together in each record:

$$\frac{C_1}{C_2} = \frac{u_2}{u_1} \qquad (4.3)$$

Where:

C_n = Calculated CO_{2ff}

u_n = Wind speed (in knots)

Over the long record in which the average wind speed dropped 10%, the CO_{2ff} record experienced a 60% increase. Therefore, the wind speed change could potentially be responsible for 10% of the change in CO_{2ff}. It could be expected that at a finer (e.g. weekly) scale, a stronger relationship between wind speed and CO_{2ff} may have been observed. However as only annual measurement is available from the tree ring sampling no further correlation can be made.

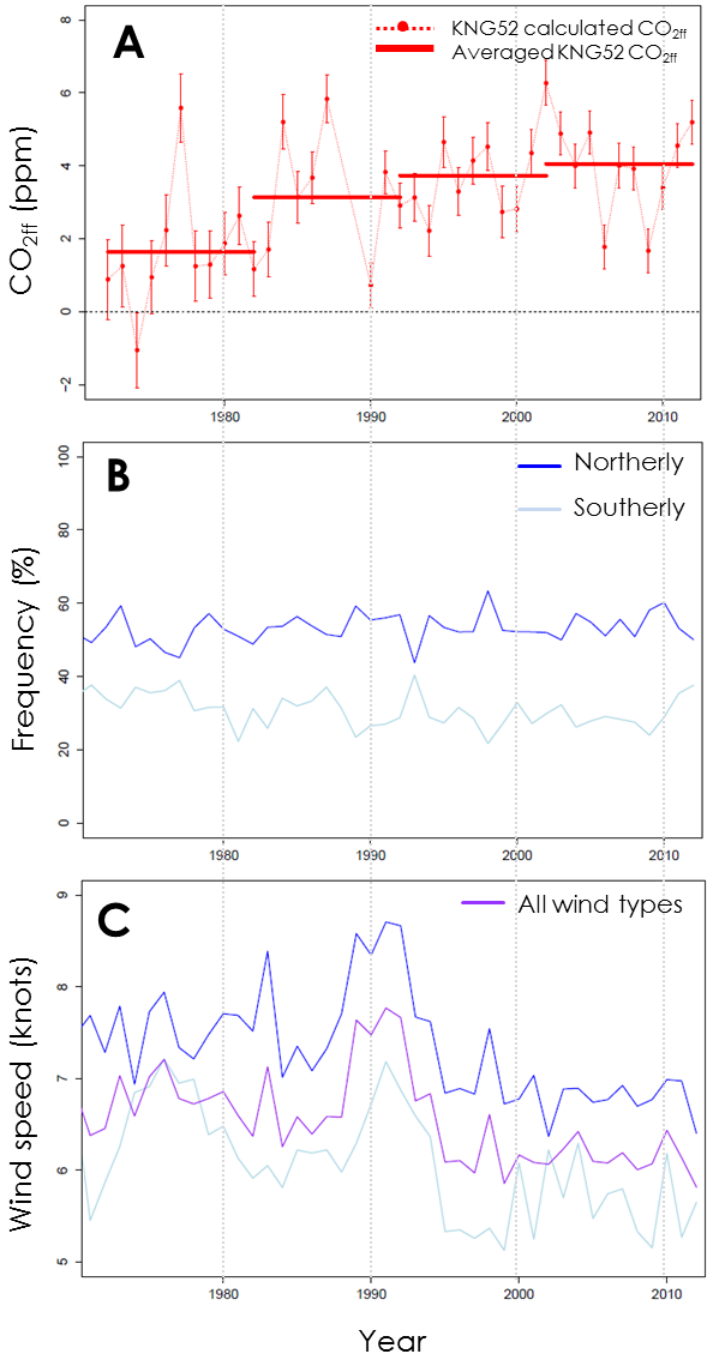

Figure 4.24: **A** – Calculated CO_{2ff} values from KNG52 $\Delta^{14}CO_2$ data. Data averaged over 10 year periods is also plotted. **B** – Wind direction frequency, very little variability occurred over the 40 year period. **C** – Average wind speed for all wind directions, Northerly only and Southerly only. There appeared to be a 10% wind speed decrease from 1970 – 1988 to 1993 – 2012.

4.4.2 Urban development

An assessment of urban development was made by observing historic aerial photos of the KNG52 test site (HCC, 2013b). Coupled with a simple analysis of the history of the central Lower Hutt region, this allowed a qualitative assessment of development and changes in traffic routes to be made. This schematic diagram represents a simplified timeline of development in the Central Lower Hutt Region (Figure 4.25).

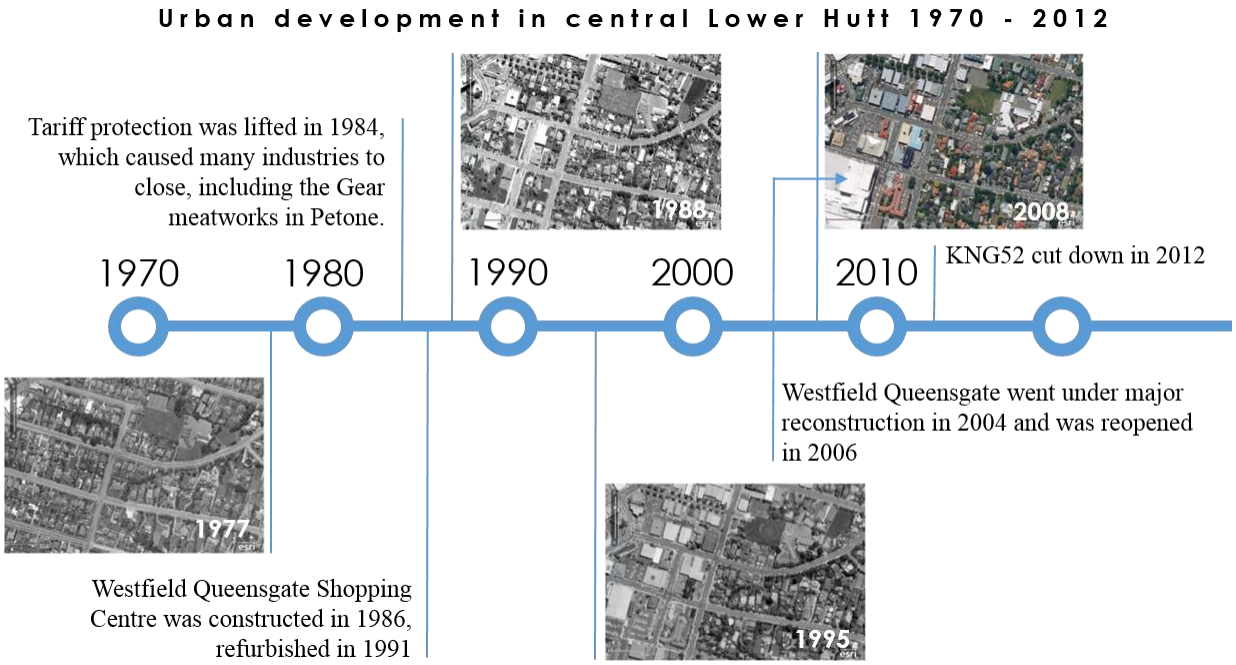

Figure 4.25: A timeline of urban development based on compiled history of events in the Lower Hutt region and historic aerial photos.

The suburbs of Petone and the Gracefield were (and the latter remains) the industrial hubs of the Lower Hutt region. Prior to the 1980s there was a railway workshop, woollen mill, meat processor and a car assembly plant. However, tariff protection was lifted in 1984, which led to a major restructuring of the industries in the area. Many industries closed, including the Gear meat works in Petone, which was replaced by a large retail precinct. However, the emissions footprint that the tree would reach is expected to be less than a 2 km radius (Kormann & Meixner, 2001). Therefore development in the Petone and Gracefield areas would not affect the KNG52 CO_{2ff} record. It is most likely that the tree would only be exposed to very local traffic and development projects.

The aerial photos reveal that there was two periods of significant urban development: 1977 to 1988 and1988 to 1995. Westfield shopping mall was constructed in 1986 and refurbished in 1991. The mall went under major reconstruction in 2004 and was reopened in 2006, which can be seen in the 2008 aerial photograph. From 2008 to 2012 there were no major reconstruction projects in the area.

A qualitative comparison of the CO_{2ff} data and the information pertaining to the local urban development revealed some possible correlation. Between the period 1977 to 1988 the aerial photos showed significant development, which complies with the significant growth in CO_{2ff} from 1972 to 1992, which increased by 112% during this period. The second period of major development between 1988 and 1995 corresponds to large variability in the record due to inconsistent sampling, as previously discussed; therefore it is difficult to make any comprehensive conclusions during this period. It was expected that there may have been an increase emissions present around the time the Westfield shopping centre was reopened in 2006 (due to increased traffic flow), however this is another period of large variability in the record, thus no comprehensive relationship is determined during this period.

This exercise showed that there may have been a relationship between periods of development and increased CO_{2ff} emissions, particularly in the period 1977 to 1988. However, due to finer scale variability in the record it is difficult to make any positive correlations. A more comprehensive investigation into traffic flow and local emissions use would help define some of this variability; however this information was not immediately available for the scale of this project.

4.5 Comparison with national emissions data

4.5.1 CDIAC data

Comprehensive traffic and fuel use data was not available for the Lower Hutt region during this period. Therefore, for further analysis of local emissions and variability seen in the KNG52 CO_{2ff} record, a comparison with national-level emissions data was made (A.4).

Emissions data were obtained from the Carbon Dioxide Information Analysis Centre (CDIAC; Boden et al., 2016). CDIAC focus on obtaining, evaluating and distributing data related to climate change and greenhouse gas emissions. The 1950 to present CO_2 emissions estimates are derived primarily from energy statistics published by the United Nations (2016), using the methods of Marland & Rotty (1984). This is the most comprehensive and accurate compilation of fossil fuel emissions on a national level. For comparison with the KNG52 CO_{2ff} data, annual concentrations of New Zealand-specific emissions from liquid sources (e.g. petrol), as well as total emissions, was obtained for the period 1972 to 2012.

The large amount of variability seen in the KNG52 data makes it difficult to make a direct comparison with the CDIAC data. Data from both sources were averaged over 10 year periods in time and plotted together to compare.

Total emissions reported by CDIAC show an 85% increase in emissions between 1972 and 2012 (Figure 4.26). Despite showing a very similar trend to that seen in the KNG52 CO_{2ff} record, this dataset is not comparable as it includes emissions sources that would not be represented in the tree CO_{2ff} record. We compare with liquid emissions only, the sources of which are largely from the traffic fleet and should be representative of fossil fuel combustion from vehicle use (the largest contribution to CO_{2ff} in Lower Hutt).

The graphics suggest overall agreement between Lower Hutt and New Zealand-wide, with liquid emissions increasing by 60% between 1972 to 2012 (Figure 4.27). Overall there is a 150% increase in emissions presented in the KNG52 record. As described earlier, the largest increase in emissions (112%) represented in the KNG52 CO_{2ff} record occurs between 1972 and 1992 - a trend that is not replicated in the CDIAC liquid emissions record. This period was characterised by extensive urban development in the Lower Hutt region, as determined by the aerial photographs (Figure 4.25. Therefore, it is possible that this rapid increase in emissions is a localised effect.

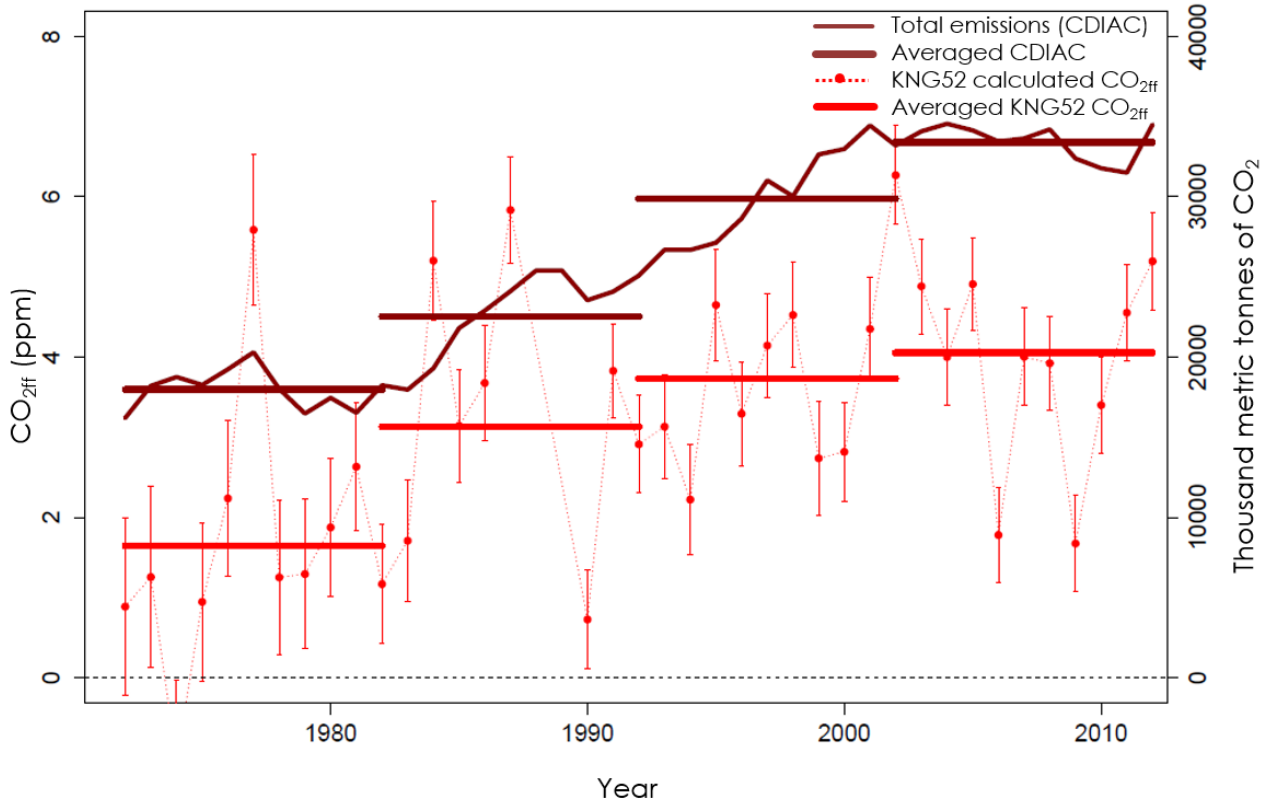

Figure 4.26: Total emissions obtained from CDIAC (Boden et al., 2016) and averaged over 10 year periods and is compared with KNG52 CO_{2ff} record.

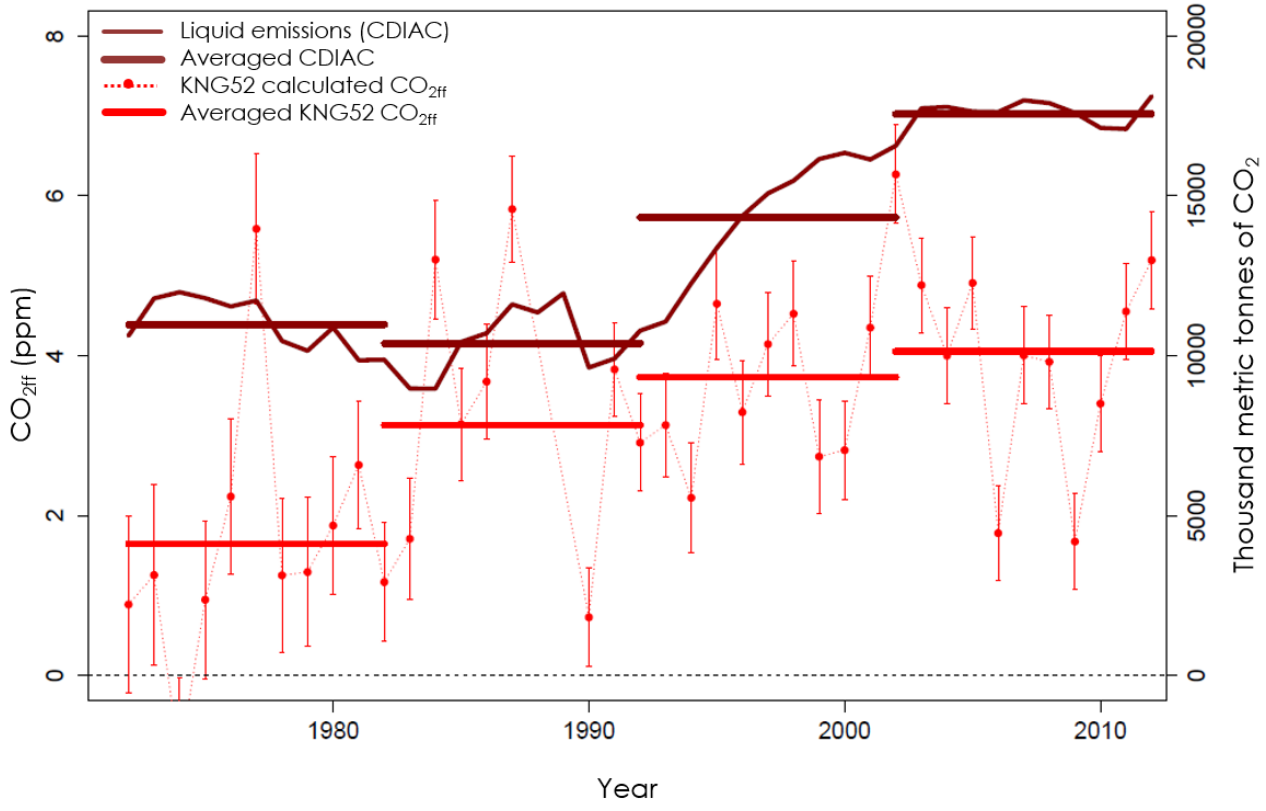

Figure 4.27: Liquid emissions from CDIAC (Boden et al., 2016) and averaged over 10 year periods and is compared with KNG52 CO_{2ff} record.

CHAPTER 5: CONCLUSIONS AND IMPLICATIONS OF RESEARCH

5.1 Research conclusions

5.1.1 $\Delta^{14}C$ change over time

This study has proven the utility of radiocarbon measurements from tree rings to reconstruct a historic record of CO_{2ff} emissions. This was achieved through the sampling of tree rings from an urban location in central Lower Hutt to provide plant material for cellulose extraction and ^{14}C measurement (KNG52). Two alternative trees were sampled at clean air locations in a coastal settlement, Eastbourne (NIK19 and NIK23). The $^{14}CO_2$ results from these trees were in general agreement with the Baring Head atmospheric record, demonstrating that the trees reliably sample atmospheric $\Delta^{14}CO_2$ concentrations.

It was hypothesised that due to its urban location, the KNG52 tree would receive local fossil fuel emissions from the surrounding area and would provide a "polluted" record of $^{14}CO_2$. The KNG52 record was compared to the BHD $^{14}CO_2$ atmospheric curve. Initial comparison showed poor agreement, particularly during the pre-bomb and bomb spike periods. This was initially thought to be a localised biospheric effect. However, shifting the chronology and re-investigating the tree ring samples identified a ring counting error. The record was amended to include the new chronology.

The radiocarbon timeline was defined by four time periods; pre-bomb, bomb period, post-bomb and fossil-era. Prior to 1960, during the pre-bomb period, a natural level of ^{14}C existed, with cosmogenic production balancing radioactive decay. A steady state of ^{14}C was accurately replicated in the KNG52 data, showing a persistent measurement of ~-25‰, likely due to cosmogenic production approximately balancing radioactive decay and the *Suess Effect.* The bomb period, characterised by a massive influx of ^{14}C into the atmosphere generated by nuclear weapons testing between 1956 and 1965, was accurately replicated. The post-bomb period, is generally characterised by rapid uptake of bomb ^{14}C by oceans and terrestrial biosphere. During this period the KNG52 record showed some variability and exhibited slightly lower values then the background records. This was reconciled by calculating the observed $^{14}CO_2$ in the absence of fossil fuels. This proved that there was a minor biospheric effect during this period, leading to lower values. From 1980s onward, during the fossil-era, additions of ^{14}C-depleted CO_{2ff} became the dominant driver of the KNG52 record.

5.1.2 CO_2ff calculation

This study included the development of a 40-year record of past CO_{2ff} emissions at the test site calculated from the $\Delta^{14}CO_2$ measurements. This calculation utilised summer-averaged BHD CO_2 and $^{14}CO_2$ concentration data to calculate CO_{2ff} of the tree ring data. It was also necessary to calculate the relative effect of biospheric respiration on the $^{14}CO_2$ signal in order to calculate the CO_{2ff} of observation years. From 1972 to 2012 the calculated CO_{2ff} values increased from 0.9 ± 1.1 ppm in 1972 to 5.2 ±0.61 ppm in 2012 with some notable variability (fluctuating between -1.05 ±1 and 6.3 ±0.6 ppm). The calculated biosphere correction showed that up until 1980 the biosphere had the effect of 'pulling up' the record. From 1980 onward, when fossil fuels became the dominant driver of CO_{2ff}, this effect was shown to reverse phase and the biosphere began 'pulling down' the record.

5.1.3 Influence of meteorology and urban development on CO_{2ff}

Strong variability in the CO_{2ff} measurements were observed throughout the record. Meteorological effects and change in urban development were observed to try to justify some of this variability.

An assessment of relative proportions of prevailing wind trajectories, average annual wind speed, and average annual wind speed for each dominant wind type was made. Results from wind trajectory analysis of the region suggested that meteorology had no significant influence on the CO_{2ff} emissions. Therefore, this was ruled out as a cause of variability in the record. Local metrological records showed a 10% decline in average wind speed from the early part of the record (1972 – 1987) to the latter part of the record (1994 – 2012). If the mole fraction increase in CO_{2ff} was solely due to the drop in wind speeds (implying an inverse relationship), then it would be expected that the magnitude in change in both records would scale together in each record. This corresponded to a marked increase of 60% in the CO_{2ff} record in this period. However this trend suggests that the wind speed change could potentially be responsible for 10% of the change in CO_{2ff}.

A qualitative comparison of historical events and urban development in the Hutt Valley region and CO_{2ff} emissions data suggested a possible increasing trend in CO_{2ff} emissions during periods of development, particularly between 1977 and 1988, although a significant relationship throughout the record was not determined.

5.1.4 Trends in CO_{2ff} observations

The calculated CO_{2ff} values calculated from the KNG52 $\Delta^{14}CO_2$ measurements were compared with reported national emissions from New Zealand (CDIAC). Emissions from liquid sources increased 60% the period 1972 to 2012, a trend that was mirrored in the KNG52 record that showed an increase of 125% the same time period.

5.1.5 Conclusions and future work

This study successfully utilised the radiocarbon method to reconstruct two retrospective records of $^{14}CO_2$ that:

1. Represented background CO_2 using a coastal located tree,
2. Strongly reflected local emissions rates based on tree rings from an urban area.

The $^{14}CO_2$ data was successfully used to quantify local CO_{2ff} emissions. The results showed that:

1. Biosphere was the dominant driver of the CO_{2ff} record prior to 1980, having the effect of 'pulling up' the record, however this effect reversed from 1980 when fossil fuel emissions became the dominant driver,
2. There was no large variability in annual wind through time, however meteorological data implied an inverse relationship between wind speed and CO_{2ff} suggesting low wind speeds were responsible for a 10% change increase in CO_{2ff},
3. Local development possibly had some relation to accelerated increases in CO_{2ff}, however no comprehensive relationship was determined,
4. Increasing liquid (road traffic) emissions were likely to be the largest driver change in observed CO_{2ff}.

Reconstructions of atmospheric fossil fuel-derived CO_2 mixing ratios from measurements of radiocarbon in tree rings is a useful and under-used method of quantifying historical CO_2 emissions in urban areas. The tree ring method was proved to be a valid and useful technique that could be applied to point source studies in conjunction with other techniques, such as CO_2 collection by absorption over NaOH solution. This technique is particularly beneficial as it allows retrospective measurements to be made, which is not able to be achieved by other techniques. This factor suggests that this method can be used to validate past emission measurements and help refine established datasets, particularly those that appear to be affected by bias in the measurements.

This approach could be especially useful for future studies aiming to characterise the heterogeneity of local emissions from the entire region of Wellington. We found that the tree rings record local

CO_{2ff}, therefore, future studies would need to select tree sites representing a variety of urban land use types or in proximity to major CO_{2ff} sources such as motorways. A variety of sites, urban and suburban, progressively more inland from the coast would project an intersection of the region and help define a coastal-inland gradient of local fossil fuel use and pinpoint sources.

REFERENCES

Baisden, W. T., Prior, C. A., Chambers, D., Canessa, S., Phillips, A., Bertrand, C., Zondervan, A., Turnbull, J. C., Kaiser, J., & Bruhn F. (2013a). Rafter radiocarbon sample preparation and data flow: Accommodating enhanced throughput and precision. Nuclear Instruments and Methods in Physics Research Section B: Beam Interactions with Materials and Atoms 294: 194-198.

Baisden, W.T. and Keller, E.D., (2013b). Synthetic constraint of soil C dynamics using 50 years of radiocarbon and Net Primary Production (NPP) in a New Zealand grassland site. Radiocarbon, 55(2–3), pp.1071-1076.

Baisden, W.T., Parfitt, R.L., Ross, C., Schipper, L.A. & Canessa, S. (2013c). Evaluating 50 years of time-series soil radiocarbon data: towards routine calculation of robust C residence times. Biogeochemistry, 112(1-3), pp.129-137.

Baisden, W.T. & Canessa, S. (2013d). Using 50 years of soil radiocarbon data to identify optimal approaches for estimating soil carbon residence times. Nuclear Instruments and Methods in Physics Research Section B: Beam Interactions with Materials and Atoms, 294, pp.588-592.

Boden, T.A., Marland, G., & Andres, R.J. (2016). Global, Regional, and National Fossil-Fuel CO_2 Emissions. Carbon Dioxide Information Analysis Center, Oak Ridge National Laboratory, U.S. Department of Energy, Oak Ridge, Tenn., U.S.A. doi 10.3334/CDIAC/00001_V2016.

Boettger, T., Haupt, M., Knöller, K., Weise, S.M., Waterhouse, J.S., Rinne, K.T., Loader, N.J., Sonninen, E., Jungner, H., Masson-Delmotte, V. & Stievenard, M. (2007). Wood cellulose preparation methods and mass spectrometric analyses of $\delta^{13}C$, $\delta^{18}O$, and nonexchangeable $\delta^{2}H$ values in cellulose, sugar, and starch: an interlaboratory comparison. Analytical Chemistry, 79(12), pp.4603-4612.

Boswijk, G., Fowler, A. M., Palmer, J. G., Fenwick, P., Hogg, A., Lorrey, A., & Wunder, J. (2014). The late Holocene kauri chronology: assessing the potential of a 4500-year record for palaeoclimate reconstruction. Quaternary Science Reviews, 90, 128-142.

Bozhinova, D., Combe, M., Palstra, S.W.L., Meijer, H.A.J., Krol, M.C. & Peters, W. (2013). The importance of crop growth modeling to interpret the $\Delta^{14}CO_2$ signature of annual plants. Global Biogeochemical Cycles, 27(3), pp.792-803.

Brailsford, G.W., Stephens, B.B., Gomez, A.J., Riedel, K., Mikaloff-Fletcher, S.E., Nichol, S.E. & Manning, M.R. (2012). Long-term continuous atmospheric CO_2 measurements at Baring Head, New Zealand.Atmospheric Measurement Techniques, 5(12), pp.3109-3117.

Broecker, W. S., Sutherland, S., Smethie, W., Peng, T. H., & Ostlund, G. (1995). Oceanic radiocarbon: Separation of the natural and bomb components. Global Biogeochemical Cycles, 9(2), 263-288.

Capano, M., Marzaioli, F., Sirignano, C., Altieri, S., Lubritto, C., D'Onofrio, A., & Terrasi, F. (2010). ^{14}C AMS measurements in tree rings to estimate local fossil CO_2 in Bosco Fontana forest (Mantova, Italy). Nuclear Instruments and Methods in Physics Research Section B: Beam Interactions with Materials and Atoms, 268(7), 1113-1116.

Ciais, P., Sabine, C., Bala, G., Bopp, L., Brovkin, V., Canadell, J., Chhabra, A., DeFries, R., Galloway, J., Heimann, M., Jones, C., Le Quéré, C., Myneni, R.B., Piao, S. & Thornton, P. (2013). Carbon and Other Biogeochemical Cycles. In: Climate Change 2013: The Physical Science Basis. Contribution of Working Group I to the Fifth Assessment Report of the

Intergovernmental Panel on Climate Change [IPCC]. Cambridge University Press, Cambridge, United Kingdom and New York, NY, USA

Cornell Tree-Ring Laboratory (2012). Corina: A file-based dendro application and the predecessor of Tellervo. Available at http://dendro.cornell.edu/corina/

Currie, K. I., Brailsford, G., Nichol, S., Gomez, A., Sparks, R., Lassey, K. R., & Riedel, K. (2011). Tropospheric $^{14}CO_2$ at Wellington, New Zealand: the world's longest record. Biogeochemistry, 104(1-3), 5-22

DECC (2013). Verification of UK Greenhouse Gas Emissions Estimates. Available at https://www.gov.uk/government/uploads/system/uploads/attachment_data/file/225523/GHG_publication29July2013.pdf

Djuricin, S., Xu, X., & Pataki, D. E. (2012). The radiocarbon composition of tree rings as a tracer of local fossil fuel emissions in the Los Angeles basin: 1980–2008. Journal of Geophysical Research: Atmospheres (1984–2012), 117(D12).

Dlugokencky, E. & Tans, P., NOAA/ESRL (2016). Trends in Atmospheric Carbon Dioxide. Available at (www.esrl.noaa.gov/gmd/ccgg/trends/)

Donahue, D.J., Linick, T.W. & Jull, A.J.T. (1990). Isotope-ratio and background corrections for accelerator mass spectrometry radiocarbon measurements. Radiocarbon, 32(2), pp.135-142.

Elsig, J, Schmitt, J., Leuenberger, D., Schneider, R., Eyer, M., Leuenberger, M., Joos, F., Fischer, H., & Stocker, T. (2009). Stable isotope constraints on Holocene carbon cycle changes from an Antarctic ice core. Nature 461 (7263) 507-510.

Fraser, P., Steele, P., Krummel, P., Allison, C., Coram, S., Dunse, B. & Vollmer, M. (2012). DSEWPaC Research Projects 2011/2012, Final Report October 2012, 14 pp., 2012a.

Fraser P, Dunse, B., Krummel, P., Steele P. & Derek, N. (2013). Australian Atmospheric Measurements and Emissions of Ozone Depleting Substances and Synthetic Greenhouse Gases, Report prepared for Department of the Environment, CSIRO Marine and Atmospheric Research, Centre for Australian Weather and Climate Research, Aspendale, Australia, iv, 42 pp.

Fritts, H.C. (1976). Tree rings and climate, 567 pp. Academic, San Diego, Calif.

GHG Protocol, (2016). GHG Protocol for Community-Scale Greenhouse Gas Emission Inventories: An Accounting and Reporting Standard for Cities. Available at http://www.ghgprotocol.org/city-accounting

Godwin, H. (1962). Half-life of radiocarbon. Nature, 195.

Graven, H.D., Gruber, N., Key, R., Khatiwala, S. and Giraud, X. (2012). Changing controls on oceanic radiocarbon: New insights on shallow-to-deep ocean exchange and anthropogenic CO2 uptake. Journal of Geophysical Research: Oceans, 117(C10).

Gurney, K.R. (2013). Beyond hammers and nails: mitigating and verifying greenhouse gas emissions. Eos, Transactions American Geophysical Union, 94(22), pp.199-199.

Gurney, K.R., Romero-Lankao, P., Seto, K.C., Hutyra, L.R., Duren, R., Kennedy, C., Grimm, N.B., Ehleringer, J.R., Marcotullio, P., Hughes, S. & Pincetl, S. (2015). Climate change: Track urban emissions on a human scale. Nature, 525, pp.179-181.

GWRC (2014). URS Report: Greenhouse Gas Inventory for the Wellington Region. Prepared for Wellington City Council by URS New Zealand Limited. Available at http://www.gw.govt.nz/assets/About-GW-the-region/Wellington-GHG-Inventory-Report-Final.pdf

GWRC (2015). Climate Change Strategy. Available at http://www.gw.govt.nz/assets/Climate-change/GWRCClimateChangeStrategy7-10-15.pdf

HCC (2013a). Aerial Photography. Available at http://gisweb.huttcity.govt.nz/Html5Viewer/?viewer=huttcity&run=Load_Aerials

HCC (2013b). Historic Aerials. Available at http://gisweb.huttcity.govt.nz/historicaerials/historicaerials.html

Hesshaimer, V., Heimann, M. & Levin, I. (1994). Radiocarbon evidence for a smaller oceanic carbon dioxide sink than previously believed. Nature,370(21), pp.201-203.

Hogg, A.G., Higham, T., Robertson, S., Beukens, R., Kankainen, T., McCormac, F.G., van der Plicht, J. & Stuiver, M. (2006). Radiocarbon age assessment of a new, near background IAEA (super 14) C quality assurance material. Radiocarbon, 37(2), pp.797-803.

Hoornweg, D., Bhada, P., Freire, M., Trejos, C.L. & Sugar, L. (2010). Cities and climate change: An urgent agenda. The World Bank, Washington, DC.

Hua, Q. & Barbetti, M. (2004). Review of tropospheric bomb ^{14}C data for carbon cycle modelling and age calibration purposes. Radiocarbon, 46(3), pp.1273-1298.

Hua, Q. & Barbetti, M. (2007). Influence of atmospheric circulation on regional $^{14}CO_2$ differences. Journal of Geophysical Research: Atmospheres, 112(D19).

Hua, Q., Barbetti, M., Jacobsen, G. E., Zoppi, U., & Lawson, E. M. (2000). Bomb radiocarbon in annual tree rings from Thailand and Australia. Nuclear Instruments and Methods in Physics Research Section B: Beam Interactions with Materials and Atoms, 172(1), 359-365.

Hua, Q., Barbetti, M., & Rakowski, A. Z. (2013). Atmospheric radiocarbon for the period 1950–2010. Radiocarbon, 55(4), 2059-2072.

IPCC (2006). IPCC Guidelines for National Greenhouse Gas Inventories, Prepared by the Greenhouse Gas Inventories Programme. B. L. Eggleston H.S., Miwa K., Ngara T. & Tanabe K. (eds). Published: IGES, Japan. Published by the Institute for Global Environmental Strategies (IGES), Hayama, Japan on behalf of the IPCC. Available at http://www.ipcc-nggip.iges.or.jp/public/2006gl/

IPCC (2013). Climate Change 2013: The Physical Science Basis. Contribution of Working Group I to the Fifth Assessment Report of the Intergovernmental Panel on Climate Change, 1535 pp., Cambridge University Press, Cambridge, United Kingdom and New York, NY, USA, doi:10.1017/CBO9781107415324.

IPCC (2014). Climate Change 2014: Synthesis Report. Contribution of Working Groups I, II and III to the Fifth Assessment Report of the Intergovernmental Panel on Climate Change [Core Writing Team, R.K. Pachauri & L.A. Meyer (eds.)]. IPCC, Geneva, Switzerland, 151 pp.

IPCC (2016). The Intergovernmental Panel on Climate Change. Available at https://www.ipcc.ch/organization/organization_history.shtml

Joos, F. & Spahni, R. (2008). Rates of change in natural and anthropogenic radiative forcing over the past 20,000 years. Proceedings of the National Academy of Sciences, 105(5), pp.1425-1430.

Kormann, R., Meixner, F.X. (2001). An analytical footprint model for non-neutral stratification. Boundary-Layer Meteorology, 99, pp.207-224.

Levin, I., Kromer, B., Schoch-Fischer, H., Bruns, M., Münnich, M., Berdau, D., Vogel, J. C. & Münnich, K. O. (1985). 25 years of tropospheric ^{14}C observations in Central Europe. Radiocarbon, 27(1), 1-19.

Levin, I., Kromer, B., Schmidt, M., & Sartorius, H. (2003). A novel approach for independent budgeting of fossil fuel CO_2 over Europe by $^{14}CO_2$ observations. Geophysical Research Letters, 30(23).

Levin, I. & Kromer, B. (2004). The tropospheric $^{14}CO_2$ level in mid latitudes of the northern hemisphere (1959-2003). Radiocarbon, 46(3), pp.1261-1271.

Levin, I., Naegler, T., Kromer, B., Diehl, M., Francey, R. J., Gomez-Pelaez, A. J., Steele, L, Wagenbach, D, Weller, R, & Worthy, D. E. (2010). Observations and modelling of the global distribution and long-term trend of atmospheric $^{14}CO_2$. Tellus B, 62(1), 26-46.

Loulergue, L., Schilt, A., Spahni, R., Masson-Delmotte, V., Blunier, T., Lemieux, B., Barnola, J.M., Raynaud, D., Stocker, T.F. & Chappellaz, J. (2008). Orbital and millennial-scale features of atmospheric CH_4 over the past 800,000 years. Nature, 453(7193).

Lüthi, D., Le Floch, M., Bereiter, B., Blunier, T., Barnola, J.M., Siegenthaler, U., Raynaud, D., Jouzel, J., Fischer, H., Kawamura, K. & Stocker, T.F. (2008). High-resolution carbon dioxide concentration record 650,000–800,000 years before present. Nature, 453(7193), pp.379-382.

Marland, G. & Rotty, R.M. (1984). Carbon dioxide emissions from fossil fuels: a procedure for estimation and results for 1950–1982. Tellus B, 36(4), pp.232-261.

Marland, G., Pielke Sr, R.A., Apps, M., Avissar, R., Betts, R.A., Davis, K.J., Frumhoff, P.C., Jackson, S.T., Joyce, L.A., Kauppi, P. & Katzenberger, J. (2003). The climatic impacts of land surface change and carbon management, and the implications for climate-change mitigation policy. Climate policy, 3(2), pp.149-157.

Marland, G., Hamal, K. & Jonas, M. (2009). How uncertain are estimates of CO_2 emissions? Journal of Industrial Ecology 13, 4-7.

Marra, M.J., Alloway, B.V. & Newnham, R.M. (2006). Paleoenvironmental reconstruction of a well-preserved Stage 7 forest sequence catastrophically buried by basaltic eruptive deposits, northern New Zealand. Quaternary Science Reviews, 25(17), pp.2143-2161.

McGavin, T. (2016). Lower Hutt (NZ) Weather. Available at http://homepages.paradise.net.nz/tmcgavin/lh_weather.html

Miller, J.B., Lehman, S. J., Montzka, S.A., Sweeney, C., Miller, B.R., Wolak, C., Dlugokencky, E.J., Southon, J.R., Turnbull, J.C. & Tans, P.P. (2012). Linking emissions of fossil fuel CO_2 and other 1547 anthropogenic trace gases using atmospheric $^{14}CO_2$. Journal of Geophysical Research 117.

Ministry for the environment (2015). New Zealand's Greenhouse Gas Inventory 1990-2013. Available at http://www.mfe.govt.nz/publications/climate-change/new-zealands-greenhouse-gas-inventory-1990-2013

Montzka, S., Reimann, S.C.L.A., O'Doherty, S., Engel, A., Krüger, K. & Sturges, W.T. (2011). Ozone-depleting substances (ODSs) and related chemicals.

New Zealand Notable Trees Trust (2008). The New Zealand Tree Register. Available at http://register.notabletrees.org.nz/. Accessed 19/06/2015

Nisbet, E., & Weiss, R. (2010). Top-down versus bottom-up. Science,328(5983), 1241-1243.

NIWA (2016). CliFlo: NIWA's National Climate Database on the Web. Available at http://cliflo.niwa.co.nz/. Retrieved 17-April-2016

Norris, M. W., Turnbull, J. C., Trimble, M., Keller, E. D., Baisden, W. T., & Renwick, J. A. (2014). Reconstruction of historic fossil CO_2 emissions using radiocarbon measurements from tree rings. In AGU Fall Meeting Abstracts.

Norris, M.W. (2015). Reconstruction of historic fossil CO_2 emissions using radiocarbon measurements from tree rings, School of Geography, Environment and Earth Sciences. Victoria University of Wellington.

Nydal, R. (1968). Further investigation on the transfer of radiocarbon in nature. Journal of Geophysical Research, 73(12), pp.3617-3635.

Palmer, J.G., Turney, C.S.M., Hogg, A.G., Lorrey, A.M. & Jones, R.J. (2015). Progress in refining the global radiocarbon calibration curve using New Zealand kauri (*Agathis australis*) tree-ring series from Oxygen Isotope Stage 3. Quaternary Geochronology, 27, pp.158-163.

Park, R. & Epstein, S. (1961). Metabolic fractionation of C^{13} & C^{12} in plants. Plant Physiology, 36(2), p.133.

Rafter, T.A. & Fergusson, G.J. (1959). Atmospheric radiocarbon as a tracer in geophysical circulation problems (No. A/CONF. 15/P/2128). Dept. of Scientific and Industrial Research, Lower Hutt, New Zealand.

Rakowski, A. Z. (2011). Radiocarbon method in monitoring of fossil fuel emission. Geochronometria, 38(4), 314-324.

Randerson, J. T., Chapin Iii, F. S., Harden, J. W., Neff, J. C., & Harmon, M. E. (2002). Net ecosystem production: a comprehensive measure of net carbon accumulation by ecosystems. Ecological applications, 12(4), 937-947.

Reimer, P.J., Baillie, M.G., Bard, E., Bayliss, A., Beck, J.W., Bertrand, C.J., Blackwell, P.G., Buck, C.E., Burr, G.S., Cutler, K.B. & Damon, P.E. (2004). IntCal04 terrestrial radiocarbon age calibration, 0-26 cal kyr BP.

Schilt, A., Baumgartner, M., Blunier, T., Schwander, J., Spahni, R., Fischer, H. & Stocker, T.F. (2010). Glacial–interglacial and millennial-scale variations in the atmospheric nitrous oxide concentration during the last 800,000 years. Quaternary Science Reviews, 29(1), pp.182-192.

Schuur, E.A.G., Trumbore, S.E., Druffel, E.R.M., Southon, J.R., Steinhof, A., Taylor, R.E. and Turnbull, J.C. (2016). Radiocarbon and the Global Carbon Cycle. In Radiocarbon and Climate Change (pp. 1-19). Springer International Publishing.

Scott, E.M. (2003). Part 2: the Third International Radiocarbon Intercomparison (TIRI). Radiocarbon, 45(2), pp.293-328.

Seto, K.C., Güneralp, B. & Hutyra, L.R. (2012). Global forecasts of urban expansion to 2030 and direct impacts on biodiversity and carbon pools. Proceedings of the National Academy of Sciences, 109(40), pp.16083-16088.

Siegenthaler, U. & Sarmiento, J.L. (1993). Atmospheric carbon dioxide and the ocean. Nature, 365(6442), pp.119-125.

Stuiver, M. & Polach, H.A. (1977). Discussion; reporting of C-14 data. Radiocarbon, 19(3), pp.355-363.

Suess, H. E. (1955). Radiocarbon concentration in modern wood. Science, 122(3166), 415-417.

Sundquist, E. T. (1986). Geologic analogs: Their value and limitations in carbon dioxide research. In The Changing Carbon Cycle (pp. 371-402). Springer New York.

Tans, P. & Keeling, R. (2016). Trends in Atmospheric Carbon Dioxide, NOAA, ESRL. Available at www.esrl.noaa.gov/gmd/ccgg/trends/

Trumbore, S.E. (1997). Potential responses of soil organic carbon to global environmental change. Proceedings of the National Academy of Sciences, 94(16), pp.8284-8291.

Turnbull, J.C. (2006a). Development of a high precision $^{14}CO_2$ measurement capability and application to carbon cycle dynamics (Doctoral thesis). University of Colorado, Boulder, Colorado, USA.

Turnbull, J. C., Miller, J. B., Lehman, S. J., Tans, P. P., Sparks, R. J., & Southon, J. (2006b). Comparison of $^{14}CO_2$, CO, and SF_6 as tracers for recently added fossil fuel CO_2 in the atmosphere and implications for biological CO_2 exchange. Geophysical research letters, 33(1).

Turnbull, J., Rayner, P., Miller, J., Naegler, T., Ciais, P., & Cozic, A. (2009). On the use of $^{14}CO_2$ as a tracer for fossil fuel CO_2: Quantifying uncertainties using an atmospheric transport model. Journal of Geophysical Research: Atmospheres (1984–2012), 114(D22).

Turnbull, J. C., Karion, A., Fischer, M. L., Faloona, I., Guilderson, T., Lehman, S. J., Miller, B. R., Montzka, S., Sherwood T., Saripalli, S., Sweeney, C. & Tans, P. P. (2011a). Assessment of fossil fuel carbon dioxide and other anthropogenic trace gas emissions from airborne measurements over Sacramento, California in spring 2009. Atmospheric Chemistry and Physics, 11(2), 705-721.

Turnbull, J. C., Tans, P. P., Lehman, S. J., Baker, D., Conway, T. J., Chung, Y. S., Gregg, J., Miller, J. B., Southon, J. R. & Zhou, L. X. (2011b). Atmospheric observations of carbon monoxide and fossil fuel CO_2 emissions from East Asia. Journal of Geophysical Research: Atmospheres (1984–2012), 116(D24).

Turnbull, J. C., Graven, H., Miller, J., & Lehman, S. (2013). Atmospheric Radiocarbon Workshop Report. Radiocarbon, 55(2–3), 1470-1474.

Turnbull, J.C., Mikaloff Fletcher, S.E., Brailsford, G.W., Currie, K.I., Moss, R.C., Steinkamp, K., Norris, M.W. & Zondervan, A. (2014a). Long-term variability in Southern Hemisphere $^{14}CO_2$ from the Wellington record, American Geophysical Union Fall Meeting. AGU, San Francisco, USA.

Turnbull, J. C., Keller, E. D., Baisden, T., Brailsford, G., Bromley, T., Norris, M., & Zondervan, A. (2014b). Atmospheric measurement of point source fossil CO_2 emissions. Atmospheric Chemistry and Physics, 14(10), 5001-5014.

Turnbull, J. C., Zondervan, A., Kaiser, J., Norris, M., Dahl, J., Baisden, T., & Lehman, S. (2015). High-Precision Atmospheric $^{14}CO_2$ Measurement at the Rafter Radiocarbon Laboratory. Radiocarbon, 57(3).

Turney, C. S., Fifield, L. K., Palmer, J. G., Hogg, A. G., Baillie, M. G., Galbraith, R., Ogden, J., Lorrey, A. & Tims, S. G. (2007). Towards a radiocarbon calibration for oxygen isotope stage 3 using New Zealand kauri (Agathis australis).

UNEP (2015). Sustainable Innovation Forum 2015: Bolstering Success in Paris. Available at http://www.cop21paris.org/

UNFCCC (1992). United Nationas Framework Convention on Climate Change. Available at https://unfccc.int/resource/docs/convkp/conveng.pdf

UNFCCC (1998). Kyoto Protocol to the United Nations Framework Convention on Climate Change. Available at http://unfccc.int/essential_background/kyoto_protocol/background/items/1351.php

UNFCCC (2015). COP21: The twenty-first session of the Conference of the Parties (COP) and the eleventh session of the Conference of the Parties serving as the meeting of the Parties to the Kyoto Protocol. (CMP). Available at http://unfccc.int/meetings/paris_nov_2015/session/9057.php

UNFCCC (2016). The Paris Agreement. Available at http://unfccc.int/paris_agreement/items/9485.php

Van Der Laan, S., Karstens, U., Neubert, R. E. M., Van Der Laan-Luijkx, I. T., & Meijer, H. A. J. (2010). Observation-based estimates of fossil fuel-derived CO_2 emissions in the Netherlands using $\Delta^{14}C$, CO and ^{222}Radon. Tellus B, 62(5), 389-402.

Zondervan, A., Hauser, T.M., Kaiser, J., Kitchen, R.L., Turnbull, J.C. & West, J.G. (2015). XCAMS: The compact ^{14}C accelerator mass spectrometer extended for ^{10}Be and ^{26}Al at GNS Science, New Zealand. Nuclear Instruments and Methods in Physics Research Section B: Beam Interactions with Materials and Atoms, 361, pp.25-33.

APPENDICES

A.1 Calculated $\Delta^{14}CO_2$ data in the absence of fossil fuels

Year	CO_{2obs}	Δ_{bg}	CO_{2bg}	Δ_r	CO_{2r}	Δff	CO_{2ff}	Δ_p	CO_{2p}	Δ_{obs1}
1959	315.04	110.07	315.04*	0.00$^+$	4.25	-1000	0	110.07	-4.25	108.59
1960	315.94	172.97	315.94*	0.00$^+$	4.25	-1000	0	172.97	-4.25	170.65
1962	316.48	204.95	316.48*	0.00$^+$	4.25	-1000	0	204.95	-4.25	202.19
1963	318.14	255.06	318.14*	0.00$^+$	4.25	-1000	0	255.06	-4.25	251.65
1964	318.72	425.03	318.72*	0.00$^+$	4.25	-1000	0	425.03	-4.25	419.36
1965	319.11	609.71	319.11*	0.00$^+$	4.25	-1000	0	609.71	-4.25	601.59
1966	320.23	637.10	320.23*	0.00$^+$	4.25	-1000	0	637.10	-4.25	628.65
1967	321.21	608.38	321.21*	0.00$^+$	4.25	-1000	0	608.38	-4.25	600.33
1968	321.99	572.73	321.99*	0.00$^+$	4.25	-1000	0	572.73	-4.25	565.17
1969	323.19	540.35	323.19*	0.00$^+$	4.25	-1000	0	540.35	-4.25	533.25
1970	324.72	522.51	324.72	0.00$^+$	4.25	-1000	0	522.51	-4.25	515.67
1971	324.74	501.18	324.74	0.00$^+$	4.25	-1000	0	501.18	-4.25	494.62
1972	325.54	482.89	325.54	-11.52	4.25	-1000	0	482.89	-4.25	476.43
1973	326.61	450.69	326.61	3.60	4.25	-1000	0	450.69	-4.25	444.87
1974	328.45	414.82	328.45	24.88	4.25	-1000	0	414.82	-4.25	409.78
1975	329.48	393.40	329.48	57.11	4.25	-1000	0	393.40	-4.25	389.06
1976	330.51	368.45	330.51	110.07	4.25	-1000	0	368.45	-4.25	365.13
1977	331.61	341.05	331.61	172.97	4.25	-1000	0	341.05	-4.25	338.90
1978	332.96	321.30	332.96	197.48	4.25	-1000	0	321.30	-4.25	319.72
1979	334.28	307.04	334.28	204.95	4.25	-1000	0	307.04	-4.25	305.75
1980	335.88	285.27	335.88	255.06	4.25	-1000	0	285.27	-4.25	284.89
1981	337.58	270.97	337.58	425.03	4.25	-1000	0	270.97	-4.25	272.91
1982	338.90	254.09	338.90	609.71	4.25	-1000	0	254.09	-4.25	258.55
1983	340.24	238.47	340.24	637.10	4.25	-1000	0	238.47	-4.25	243.45
1984	341.87	224.06	341.87	608.38	4.25	-1000	0	224.06	-4.25	228.84
1985	342.83	210.50	342.83	572.73	4.25	-1000	0	210.50	-4.25	214.99
1986	344.32	200.99	344.32	540.35	4.25	-1000	0	200.99	-4.25	205.18
1987	345.92	187.97	345.92	522.51	4.25	-1000	0	187.97	-4.25	192.08
1990	351.30	155.21	351.30	450.69	4.25	-1000	0	155.21	-4.25	158.78
1991	352.59	147.48	352.59	414.82	4.25	-1000	0	147.48	-4.25	150.70
1992	353.55	140.40	353.55	393.40	4.25	-1000	0	140.40	-4.25	143.44
1993	354.88	133.93	354.88	368.45	4.25	-1000	0	133.93	-4.25	136.74
1994	355.66	127.46	355.66	341.05	4.25	-1000	0	127.46	-4.25	130.01
1995	356.82	122.78	356.82	321.30	4.25	-1000	0	122.78	-4.25	125.15
1996	359.36	113.69	359.36	307.04	4.25	-1000	0	113.69	-4.25	115.98
1997	360.55	111.99	360.55	285.27	4.25	-1000	0	111.99	-4.25	114.03
1998	362.30	107.01	362.30	270.97	4.25	-1000	0	107.01	-4.25	108.93
1999	364.81	100.91	364.81	254.09	4.25	-1000	0	100.91	-4.25	102.69
2000	365.98	91.23	365.98	238.47	4.25	-1000	0	91.23	-4.25	92.94
2001	367.52	90.16	367.52	224.06	4.25	-1000	0	90.16	-4.25	91.71
2002	368.39	87.61	368.39	210.50	4.25	-1000	0	87.61	-4.25	89.02
2003	371.51	82.94	371.51	200.99	4.25	-1000	0	82.94	-4.25	84.29
2004	373.64	76.65	373.64	187.97	4.25	-1000	0	76.65	-4.25	77.91
2005	375.47	71.63	375.47	177.24	4.25	-1000	0	71.63	-4.25	72.83
2006	377.77	62.00	377.77	170.17	4.25	-1000	0	62.00	-4.25	63.22
2007	379.41	59.36	379.41	155.21	4.25	-1000	0	59.36	-4.25	60.44
2008	381.54	55.81	381.54	147.48	4.25	-1000	0	55.81	-4.25	56.83
2009	383.44	51.13	383.44	140.40	4.25	-1000	0	51.13	-4.25	52.12
2010	384.86	49.76	384.86	133.93	4.25	-1000	0	49.76	-4.25	50.69
2011	387.48	46.09	387.48	127.46	4.25	-1000	0	46.09	-4.25	46.99
2012	388.67	37.14	388.67	122.78	4.25	-1000	0	37.14	-4.25	38.08

*Denotes CO_2 concentration data accessed from Mauna Loa record (Tans & Keeling, 2016; BHD CO_2 record starts in 1970). The Mauna Loa data is not seasonally adjusted for Southern hemisphere conditions. The Baring Head CO_2 concentration record accessed from NIWA website was averaged for the September April period (Brailsford et al. 2012; NIWA, 2016)

The BHD $^{14}CO_2$ data (Δ_{bg}) is the result of a smooth fit analysis (Turnbull eta., 2014a), this was averaged for the months September to April to create an annual value.

$^{+}$ Δ_r data was not available prior to 1970, thus was assumed to be 0 prior to this.

A.2 CO_{2ff} emissions calculated from KNG52 $^{14}CO_2$ record

Year	CO_2 (ppm)	CO_2 (s.d.)	BHD ^{14}C	BHD ^{14}C error	KNG52 ^{14}C	KNG ^{14}C err	Δ_{ff}	CO_{2ff}	CO_{2ff} error
1972	325.54	0.18	482.89	1.73	472.53	3.05	-1000	2.27	0.98
1973	326.61	0.5	450.69	2.14	439.36	2.98	-1000	2.55	1.01
1974	328.45	0.38	414.82	1.52	414.31	2.93	-1000	0.12	0.92
1975	329.48	0.24	393.40	1.43	385.17	2.9	-1000	1.95	0.90
1976	330.51	0.27	368.45	1.57	356.04	2.83	-1000	3.00	0.90
1977	331.61	0.25	341.05	1.65	316.45	2.77	-1000	6.08	0.90
1978	332.96	0.24	321.30	1.95	314.89	2.78	-1000	1.62	0.94
1979	334.28	0.55	307.04	1.77	300.83	2.74	-1000	1.59	0.91
1980	335.88	0.23	285.27	1.45	277.76	2.67	-1000	1.96	0.85
1981	337.58	0.24	270.97	1.43	263.07	2.66	-1000	2.10	0.84
1982	338.90	0.28	254.09	1.58	254.3	2.63	-1000	-0.06	0.85
1983	340.24	0.14	238.47	1.81	237.31	2.6	-1000	0.32	0.88
1984	341.87	0.08	224.06	1.75	210.32	2.59	-1000	3.84	0.87
1985	342.83	0.42	210.50	1.50	204.04	2.54	-1000	1.83	0.82
1986	344.32	0.22	200.99	1.580	192.57	2.53	-1000	2.41	0.83
1987	345.92	0.33	187.97	1.14	172.22	2.51	-1000	4.59	0.77
1990	351.30	0.2	155.21	0.81	156.44	2.44	-1000	-0.37	0.71
1991	352.59	0.29	147.48	0.61	138.31	2.41	-1000	2.82	0.68
1992	353.55	0.77	140.40	0.73	134.14	2.41	-1000	1.94	0.69
1993	354.88	0.61	133.93	1.06	126.84	2.41	-1000	2.22	0.73
1994	355.66	0.14	127.46	1.14	123.09	2.495	-1000	1.38	0.77
1995	356.82	0.42	122.78	1.37	110.66	2.37	-1000	3.85	0.76
1996	359.36	0.15	113.69	1.07	105.88	2.34	-1000	2.52	0.72
1997	360.55	0.3	111.99	0.98	101.4	2.34	-1000	3.43	0.71
1998	362.30	0.52	107.01	1.04	95.24	2.35	-1000	3.85	0.72
1999	364.81	0.21	100.91	1.51	94.55	2.31	-1000	2.11	0.77
2000	365.98	0.17	91.23	0.79	84.62	2.29	-1000	2.22	0.67
2001	367.52	0.18	90.16	0.94	78.96	2.3	-1000	3.78	0.69
2002	368.39	0.24	87.61	0.73	70.71	2.29	-1000	5.72	0.66
2003	371.51	0.39	82.94	0.54	70.24	2.29	-1000	4.36	0.64
2004	373.64	0.3	76.65	0.51	66.53	2.31	-1000	3.51	0.64
2005	375.47	0.15	71.63	0.50	58.95	2.24	-1000	4.44	0.62
2006	377.77	0.29	62.00	0.55	58.3	2.27	-1000	1.32	0.64
2007	379.41	0.38	59.36	0.67	49.36	2.26	-1000	3.58	0.65
2008	381.54	0.13	55.81	0.49	46.07	2.22	-1000	3.52	0.62
2009	383.44	0.4	51.13	0.56	47.6	2.25	-1000	1.29	0.63
2010	384.86	0.16	49.76	0.57	41.53	2.24	-1000	3.02	0.63
2011	387.48	0.63	46.09	0.60	34.84	2.24	-1000	4.17	0.64
2012	388.67	0.25	37.14	0.59	24.31	2.28	-1000	4.81	0.64

A.3 CO_{2ff} emissions biosphere correction

Year	KNG52 ^{14}C	KNG ^{14}C err	CO_{2ff}	CO_{2ff} error	CO_{2r}	Δ_r	Δ_r error	Δ_{ff}	CO_{2ff}	CO_{2ff} error	CO_{2ff1}	CO_{2ff1} error
1972	472.53	3.05	2.27	0.98	4.25	-11.52	3.24	-1000	2.27	0.98	2.27	0.98
1973	439.36	2.98	2.55	1.01	4.25	3.60	2.25	-1000	2.55	1.01	2.55	1.01
1974	414.31	2.93	0.12	0.92	4.25	24.88	1.70	-1000	0.12	0.92	0.12	0.92
1975	385.17	2.9	1.95	0.90	4.25	57.11	1.57	-1000	1.95	0.90	1.95	0.90
1976	356.04	2.83	3.00	0.90	4.25	110.07	1.68	-1000	3.00	0.90	3.00	0.90
1977	316.45	2.77	6.08	0.90	4.25	172.97	2.02	-1000	6.08	0.90	6.08	0.90
1978	314.89	2.78	1.62	0.94	4.25	197.48	2.08	-1000	1.62	0.94	1.62	0.94
1979	300.83	2.74	1.59	0.91	4.25	204.95	3.04	-1000	1.59	0.91	1.59	0.91
1980	277.76	2.67	1.96	0.85	4.25	255.06	2.48	-1000	1.96	0.85	1.96	0.85
1981	263.07	2.66	2.10	0.84	4.25	425.03	1.77	-1000	2.10	0.84	2.10	0.84
1982	254.3	2.63	-0.06	0.85	4.25	609.71	2.39	-1000	-0.06	0.85	-0.06	0.85
1983	237.31	2.6	0.32	0.88	4.25	637.10	1.97	-1000	0.32	0.88	0.32	0.88
1984	210.32	2.59	3.84	0.87	4.25	608.38	2.07	-1000	3.84	0.87	3.84	0.87
1985	204.04	2.54	1.83	0.82	4.25	572.73	1.79	-1000	1.83	0.82	1.83	0.82
1986	192.57	2.53	2.41	0.83	4.25	540.35	1.51	-1000	2.41	0.83	2.41	0.83
1987	172.22	2.51	4.59	0.77	4.25	522.51	1.87	-1000	4.59	0.77	4.59	0.77
1990	156.44	2.44	-0.37	0.71	4.25	450.69	2.14	-1000	-0.37	0.71	-0.37	0.71
1991	138.31	2.41	2.82	0.68	4.25	414.82	1.52	-1000	2.82	0.68	2.82	0.68
1992	134.14	2.41	1.94	0.69	4.25	393.40	1.43	-1000	1.94	0.69	1.94	0.69
1993	126.84	2.41	2.22	0.73	4.25	368.45	1.57	-1000	2.22	0.73	2.22	0.73
1994	123.09	2.495	1.38	0.77	4.25	341.05	1.65	-1000	1.38	0.77	1.38	0.77
1995	110.66	2.37	3.85	0.76	4.25	321.30	1.95	-1000	3.85	0.76	3.85	0.76
1996	105.88	2.34	2.52	0.72	4.25	307.04	1.77	-1000	2.52	0.72	2.52	0.72
1997	101.4	2.34	3.43	0.71	4.25	285.27	1.45	-1000	3.43	0.71	3.43	0.71
1998	95.24	2.35	3.85	0.72	4.25	270.97	1.43	-1000	3.85	0.72	3.85	0.72
1999	94.55	2.31	2.11	0.77	4.25	254.09	1.58	-1000	2.11	0.77	2.11	0.77
2000	84.62	2.29	2.22	0.67	4.25	238.47	1.81	-1000	2.22	0.67	2.22	0.67
2001	78.96	2.3	3.78	0.69	4.25	224.06	1.75	-1000	3.78	0.69	3.78	0.69
2002	70.71	2.29	5.72	0.66	4.25	210.50	1.50	-1000	5.72	0.66	5.72	0.66
2003	70.24	2.29	4.36	0.64	4.25	200.99	1.58	-1000	4.36	0.64	4.36	0.64
2004	66.53	2.31	3.51	0.64	4.25	187.97	1.14	-1000	3.51	0.64	3.51	0.64
2005	58.95	2.24	4.44	0.62	4.25	177.24	1.12	-1000	4.44	0.62	4.44	0.62
2006	58.3	2.27	1.32	0.64	4.25	170.17	1.11	-1000	1.32	0.64	1.32	0.64
2007	49.36	2.26	3.58	0.65	4.25	155.21	0.81	-1000	3.58	0.65	3.58	0.65
2008	46.07	2.22	3.52	0.62	4.25	147.48	0.61	-1000	3.52	0.62	3.52	0.62
2009	47.6	2.25	1.29	0.63	4.25	140.40	0.73	-1000	1.29	0.63	1.29	0.63
2010	41.53	2.24	3.02	0.63	4.25	133.93	1.06	-1000	3.02	0.63	3.02	0.63
2011	34.84	2.24	4.17	0.64	4.25	127.46	1.14	-1000	4.17	0.64	4.17	0.64
2012	24.31	2.28	4.81	0.64	4.25	122.78	1.37	-1000	4.81	0.64	4.81	0.64

A.4 Emissions of CO_{2ff} data reported CDIAC

Year	Total emissions CDIAC	Liquid emissions CDIAC
1972	16197.14	10623.30
1973	18202.99	11793.07
1974	18756.71	11987.42
1975	18261.66	11800.41
1976	19237.08	11540.05
1977	20300.51	11723.40
1978	18008.64	10461.95
1979	16475.83	10153.92
1980	17458.59	10883.66
1981	16527.17	9856.90
1982	18239.66	9871.56
1983	17964.63	8973.15
1984	19295.75	8969.48
1985	21803.98	10428.95
1986	22893.08	10703.97
1987	24110.53	11606.06
1988	25397.64	11353.03
1989	25404.98	11950.75
1990	23545.81	9629.54
1991	24084.86	9908.23
1992	25082.28	10780.98
1993	26688.43	11067.01
1994	26681.09	12262.45
1995	27132.13	13369.88
1996	28642.94	14374.64
1997	31022.82	15078.70
1998	30029.06	15474.74
1999	32639.97	16153.14
2000	32981.00	16347.49
2001	34447.80	16138.47
2002	33201.02	16571.17
2003	34081.10	17740.95
2004	34554.14	17781.28
2005	34139.77	17638.27
2006	33446.71	17623.60
2007	33637.39	17990.30
2008	34202.11	17902.29
2009	32386.94	17597.93
2010	31778.22	17128.56
2011	31503.20	17091.89
2012	34506.47	18118.65